

Improving Predictions for Helium Emission Lines

Robert A. Benjamin¹

University of Wisconsin-Madison, Dept. of Physics, 1150 University Avenue, Madison, WI 53706;
benjamin@wisp.physics.wisc.edu

Evan D. Skillman

Department of Astronomy, University of Minnesota, Minneapolis, MN 55455; skillman@ast1.spa.umn.edu

Derck P. Smits

Dept Math & Astronomy, University of South Africa, PO Box 392, Pretoria 0003 South Africa;
dps@pc-2029227.unisa.ac.za

ABSTRACT

We have combined the detailed He I recombination model of Smits with the collisional transitions of Sawey & Berrington in order to produce new accurate helium emissivities that include the effects of collisional excitation from both the 2^3S and 2^1S levels. We present a grid of emissivities for a range of temperature and densities along with analytical fits and error estimates. These grids eliminate the necessity of making corrections for collisional enhancements as in the work of Clegg or Kingdon & Ferland for lines with upper levels below $n=5$. For densities greater than $n_e \approx 10^6 \text{ cm}^{-3}$, inclusion of collisional excitation from the 2^1S level is also necessary if accuracies of greater than a few percent are required.

Atomic data for a model atom with 29 levels ($n_{max} = 5$) is presented which matches the recombination model of Smits to within 5% over the temperature range $T = 5000 - 20000 \text{ K}$. Using the algorithm of Almog & Netzter, collisional effects are calculated self-consistently. This model atom will be useful in models of radiative transfer. A notable feature of this technique is an algorithm which calculates the “indirect” recombination rates, the recombination to individual levels which go through $n > n_{max}$ first.

Fits accurate to within 1% are given for the emissivities of the brightest lines over a restricted range for estimates of primordial helium abundance. We characterize the analysis uncertainties associated with uncertainties in temperature, density, fitting functions, and input atomic data. We estimate that atomic data uncertainties alone may limit abundance estimates to an accuracy of $\sim 1.5\%$; systematic errors may be greater than this. This analysis uncertainty must be incorporated when attempting to make high accuracy estimates of the helium abundance. For example, in recent determinations of the primordial helium abundance, uncertainties in the input atomic data have been neglected.

Finally, we compare our theoretical calculations to the measured strengths of a few dozen helium emission lines in three nebulae, Orion (NGC 1976) and the planetary nebulae, NGC 6572 and IC 4997. Incorporation of collisional effects yields noticeable improvements for some lines, but some notable discrepancies remain.

1. Motivation

¹Previous address: Minnesota Supercomputer Institute, 1200 Washington Ave, SE, Minneapolis, MN 55415

The majority of helium was created in the first few minutes of the Universe’s existence and was first discovered in 1868 (Lockyer 1868) as an emission line at 5876 Å in the spectrum of a solar prominence. Since then it has become clear that measuring the abundance of helium in astrophysical objects can be used to constrain the parameters of primordial nucleosynthesis (see Walker et al 1991). Helium abundance is a particularly useful diagnostic, since unlike deuterium and lithium, its abundance only increases with time. Measurement of accurate helium abundances in low abundance objects sets a firm upper limit on the primordial helium abundance, and extrapolation of the helium abundance down to zero metallicity can be used to estimate the primordial helium abundance (Peimbert & Torres-Peimbert 1974).

While the monotonic change of helium abundance with time is useful, the variation of the primordial value of the helium abundance with cosmological parameters is sufficiently small that extremely accurate measurements of the helium abundance are required to provide useful cosmological constraints. This requires precise measurements of helium emission lines and accurate models of the recombination spectrum of helium and an understanding of the uncertainties in both. Previously it has been assumed that the uncertainties associated with the recombination model were significantly less than the observational uncertainties. However, with observations now able to determine helium abundance to within $\sim 2\%$ (Skillman et al. 1994), it has become necessary to revisit this assumption. Improving the recombination model and assessing the uncertainties is the focus of this paper. In addition to being useful for constraining helium abundances, an accurate recombination model is also useful for providing constraints on nebular parameters such as optical depths, temperatures, and extinction.

Numerous authors have calculated the recombination spectrum of neutral helium (Mathis 1957; Burgess & Seaton 1960a,b; Pottasch 1961; Robbins 1968; Robbins 1970; Robbins & Robinson 1971; Bhatia & Underhill 1985; Brocklehurst 1972; Almog & Netzer 1989; Smits 1991b,1996). The calculations over this span have been characterized by improvements in atomic data, an increase in accuracy as more levels can be accurately included, and the rooting out of occasional bugs or inaccurate approximations. The most accurate treatment of emissivities from the helium atom in nebular environment currently available is that of Smits (1996). This work used the most accurate calculations of spontaneous radiative transitions to date (Kono & Hattori 1984), which supersedes the compilation of Wiese, Smith & Glennon (1966). It also recalculated the radiative recombination rates for several levels using updated He I photoionization cross sections of Fernley et al (1987). In addition, it corrects an error in Brocklehurst (1972) affecting the $2^3P - n^3S$ series and an error affecting high temperature recombination rates in Smits (1991b).

With accuracies of a few percent required, it has also been found that collisional excitation from the metastable 2^3S plays a significant role for several bright lines, even at the low densities characteristic of extragalactic H II regions. Twice in the past (Cox & Daltabuit 1971; Ferland 1986) it has been suggested that high values of collisional excitation rates might force a significant re-evaluation of derived helium abundances, although in both cases it turned out that the collisional rates were overestimates. In order to constrain these collisional corrections to the radiative cascade, quantum calculations of increasing accuracy have been carried out to determine more exact collisional rates (Berrington et al. 1985; Berrington & Kingston 1987; Sawey & Berrington 1993).

2. A New Model Helium Atom

Here, we present calculations of helium emission which combine the recombination and radiative cascade data of Smits (1996, hereafter S96) with the collisional rates of Sawey & Berrington (1993, hereafter

SB93). Using a similar algorithm to that used by Almog & Netzer (1989, hereafter AN89), we construct model helium atoms with a small number of levels which match the calculations of S96 to within less than 0.2% for $n_e \leq 10^6 \text{ cm}^{-3}$. These calculations are valuable for two reasons. First, since collisional effects are completely and self-consistently included in these calculations, it eliminates the need to estimate collisional correction factors for emission line intensities, as in Clegg (1987) or Kingdon & Ferland (1995, hereafter KF95). And second, the small but accurate model atom presented here can then be used in a model of radiative transfer which will allow these models to be calculated rapidly without a loss in accuracy for prediction of emission line intensities.

2.1. Atomic Data

The data used here are described in SB93, S96 and references therein, and are summarized in the Appendix A. The values for a $n_{max} = 5$ model helium atom is given in Tables 1-4. In these tables we present power-law fitting functions for the temperature dependent rates. For example, the recombination rate to an individual level is given by $\alpha_{nl}(T) = \alpha_4 t^{b\alpha}$, where $t \equiv T/10^4 \text{ K}$. For all rates, the power-law is chosen such that at $t = 1$ the agreement with our calculations is exact. We also tabulate $\pm e_\alpha$, the maximum percentage error associated with the fits over the temperature range $t = 0.5 - 2.0$. We also give fits to the *total* Case B recombination rates into the singlet and triplet ladders. Table 2 contains fits for the three body recombination rates, given by $\alpha^{tbr} = \alpha_4^{tbr} t^{b\alpha^{tbr}}$, and the fits to the collisional ionization rate, $C^{ion} = at^b e^{c/t}$. For temperatures outside this range, for applications which require a higher degree of accuracy, and for data for larger model atoms, readers should contact the authors for an extensive grid of rates.

Note that by using fits to the atomic data rather than the original atomic data themselves, the resulting calculations will be slightly less accurate. Over the temperature range $t = 0.5 - 2.0$, the line fluxes derived using the data in Tables 1-4 are accurate to within 9.6% for $n_e < 10^8 \text{ cm}^{-3}$, and accurate to within 6.1% for $n_e < 10^6 \text{ cm}^{-3}$. In all results reported here, we use the original atomic data rather than the fitting functions given in the tables.

Although we have incorporated all of the collisional transitions in our calculations, numerical experimentation described below has shown that for densities as high as $n_e = 10^8 \text{ cm}^{-3}$, only collisional transitions from 2^1S and 2^3S and those with $\Delta n = 0$ affect the predicted line fluxes. The effects of turning on all other collisions changes the line fluxes by less than 0.01 %. However we include all collision strengths in Table 4.

We can match the $N \sim 3000$ level calculation of S96 with only $N = 29$ levels (for $n_{max} = 5$) using an algorithm which calculates the “indirect recombination” rate, $\alpha'(n_e, T)$, from levels above n_{max} into the individual levels of our model atom. These rates are in Table 3. They have a weak density dependence since the recombination cascade in the levels above n_{max} is affected by collisional mixing. Below $n_{e,2} \equiv n_e/10^2 \text{ cm}^{-3} = 1$, the indirect recombination rates have negligible density dependence and are fit by $\alpha' = \alpha'_4 t^{b\alpha'}$, while above this density we use $\alpha' = \alpha'_4 t^{b\alpha'} n_{e,2}^{c\alpha'}$. Holding the density fixed at $n_e = 10^2 \text{ cm}^{-3}$, the maximum percentage error associated with this fit over the temperature range $t = 0.5 - 2.0$ is $e_{\alpha'}(n_e)$. Holding the temperature fixed at $t = 1$, the maximum error over the density range $n_e = 10^2 - 10^6 \text{ cm}^{-3}$ is $e_{\alpha'}(T)$. For the $n_{max} = 5$ atom presented here, the indirect recombination rate to most levels ranges from 20 % to 50 % of the sum of the indirect and direct rates.

The indirect recombination rates account for recombination that passes through levels greater than

n_{max} , where n_{max} is the upper cutoff for the model atom. In previous works, such as AN89 and Cota (1987), the upper levels have been replaced by one or two “fictional” level with a set of A -values from these levels. However, no attempts were made to “tune” the A -values from the “fictional” levels such that the population of given level with $n < n_{max}$ exactly matches the value that it would have had in the general case. For the purposes here, we needed a more accurate algorithm.

We calculate the indirect recombination as follows. Following Osterbrock (1989), we define the probability and cascade matrices, \mathbf{P} and \mathbf{C} where

$$P_{i,k} \equiv A_{i,k} / \sum_{E_i > E_j} A_{i,j} , \quad (1)$$

is the probability that the population of level i will be followed by a radiative decay to level k . The elements of the cascade matrix are

$$C_{i,k} \equiv \sum_{E_i > E_j > E_k} C_{i,j} P_{j,k} , \quad (2)$$

which gives the probability that the population of i will eventually yield a transition to level k via all intermediate routes j , where it is assumed that $C_{i,i} \equiv 1$.

For a pure radiative cascade, the population n_k of a level k is set by balancing the rates for population and de-population. The depopulation rate is the sum all possible radiative decays, i.e. $\sum_l A_{k,l}$ where $E_k > E_l$. The population rate consists of three terms: (1) direct recombination rate to level k , $n_e \alpha_k$, (2) direct recombination to all included upper levels i followed by a cascade to level k , $\sum_i n_e \alpha_i C_{i,k}$, and (3) the indirect recombination, $n_e \alpha'_k$.

If n_k is the population of level k as derived by the full calculation of S96, one can solve for the indirect recombination rate

$$n_e n_{He^+} \alpha'_k = n_k \sum_l A_{k,l} - n_e n_{He^+} \sum_i (\alpha_i + \alpha'_i) C_{i,k} . \quad (3)$$

This relation can be solved for successively from the highest energy level to the lowest. This formulation allows us to match the level populations of S96 exactly with a finite number of levels, so long as collisional processes are negligible in determining the level populations. Note that the sum of all indirect and direct recombination rates should equal the total recombination rate; we have checked to verify this and found it to be true within 2% for $n_e \leq 10^6$, and 10 % for $n_e = 10^8 \text{ cm}^{-3}$. We have also used these indirect recombination rates with the data otherwise identical to those of S96 and found that the level populations from our model atom agree with the calculation of S96 to better than 0.2% for $n_e \leq 10^6$. Note that in this test, although our data is identical to that of Smits (1996), the numerical method used to calculate the level populations, described in the next section, is independent.

It should be noted that this “indirect” recombination rate is different from the “effective” recombination rate for a given level, as in Osterbrock (1989), since the effective recombination rate to a given level will also include the cascade from levels $n \leq 5$, as well as the direct and indirect recombination. The effective recombination rate may be calculated using the emissivities in Table 5-7 together with the A -values in Table 4.

3. Emissivities

Because of the coupling of the singlet and triplet levels via collisional routes, we use a matrix inversion routine to solve for the level populations and the resultant emissivities. The equation of statistical equilibrium for a level k ,

$$n_e n_{He^+} [\alpha_k(T) + \alpha'_k(T, n_e) + n_e \alpha_k^{tbr}(T)] + \sum_{E_i > E_k} n_i A_{i,k} + \sum_X \sum_j n_X n_j q_{j,k}^X = n_k \left[n_e C_k^{ion} + \sum_{E_k > E_l} A_{k,l} + \sum_X \sum_j n_X q_{k,j}^X \right], \quad (4)$$

can be used to calculate the populations for $k_{max} = n_{max}(n_{max} + 1) - 1$ levels, where n_{max} is the maximum principal quantum number for the model atom. The collisional transitions with species $X = e, p, He^+$ and radiative decay from 2^3S to 1^1S can couple the singlet ($S = 0, g_S = 1$) and triplet ($S = 1, g_S = 3$) recombination ladders, so that level populations for both ladders must be solved simultaneously. The index of an individual level characterized by quantum numbers n, l , and S is $K = 2[n(n-1)/2 + l] + (1 - S)$.

These equations are solved in the Case B limit, in which photons associated with all permitted radiative transitions to 1^1S are assumed to be reabsorbed. In Case B, all electric dipole transitions to 1^1S and α_1 are set to zero.

Because of the collisional coupling between the singlet and triplet ladders, we can not apply a simple iterative scheme to determine the level populations as in Brocklehurst (1972) or Smits(1991a). Instead, we use the same algorithm as AN89. This involves expressing the rate equations in matrix form: $\mathbf{R} \cdot \mathbf{n} = \alpha$, where

$$\begin{pmatrix} -\Gamma + n_e \mathcal{Q}_1 + n_e C_1^{ion} & A_{2,1} + n_e q_{2,1} & \dots & A_{k_{max},1} + q_{k_{max},1} \\ n_e q_{1,2} & -(\mathcal{A}_2 + n_e \mathcal{Q}_2 + n_e C_2^{ion}) & \dots & A_{k_{max},2} + q_{k_{max},2} \\ \vdots & \vdots & \ddots & \vdots \\ n_e q_{1,k_{max}} & n_e q_{2,k_{max}} & \dots & -(\mathcal{A}_{k_{max}} + n_e \mathcal{Q}_{k_{max}} + n_e C_{k_{max}}^{ion}) \end{pmatrix} \mathbf{n} = -n_e n_{He^+} \alpha^{\text{tot}} \quad (5)$$

$\mathbf{n} = (n_1, \dots, n_{k_{max}})$ is the vector of level populations and $\alpha^{\text{tot}} = (\alpha_1^{\text{tot}}, \dots, \alpha_{k_{max}}^{\text{tot}})$ is the vector of recombination rates, where $\alpha_k^{\text{tot}} = \alpha_k + \alpha'_k + n_e \alpha_k^{tbr}$.

In the rate matrix, the collisional rate coefficient is $q_{k,j} = \sum_X (n_X/n_e) q_{k,j}^X$, and Γ (s^{-1}) is the photoionization rate from the ground state. Here it is assumed that the levels have been rearranged such that the index increases monotonically with energy, i.e., $k_2 > k_1$ implies $E_{k_1} > E_{k_2}$. The diagonal elements of \mathbf{R} are the depopulation rates from a given level due to radiative decays ($\mathcal{A} = \sum_l A_{k,l}$), collisional transitions ($\mathcal{Q} = \sum_X \sum_j n_X q_{k,j}$), and collisional ionization ($n_e C_k^{ion}$). The entries above the diagonal are the decays, the entries below are the excitations, and the right hand matrix contains the population rates of each level due to recombination. This matrix will be sparse, since many of the elements are zero. For

example, singlet and triplet energy levels are only coupled by three radiative decay routes; A_{k_1, k_2} 's are zero unless $l_{k_1} = l_{k_2} \pm 1$, and so on.

Inversion of \mathbf{R} using a standard numerical routine for matrix inversion (Press et al. 1986) allows one to solve for the matrix of level populations n . If there were no coupling between singlet and triplets, the matrix could be broken into two independent submatrices and solved faster. In the limit of a pure radiative cascade ($n_e \rightarrow 0$) with no forbidden transitions, the matrix will become singular, since there are no depopulation mechanisms for the 2^1S or 2^3S levels. In this limit, the rows and columns in the above matrix equation corresponding to these levels must be removed.

Using these level populations, we calculate the line emissivities. Tables 5-7 give the emission coefficient, $4\pi j_{line}/n_e n_{He+}$, for the He I emission line at 4471 Å for a range of temperature and densities. For convenience we also include the He II 4686 Å line, and hydrogen $H\beta$ and $Br\gamma$ lines calculated by Storey & Hummer (1995). We give the ratio of emissivities for all emission lines with $j_{line}/j_{4471} > 10^{-2}$. However, this table only includes lines originating from levels $n \leq 5$ with $\lambda < 2.5\mu m$. The wavelengths of the lines are those calculated using the energy levels of Table 1, and will differ from wavelengths observed in air, e.g., the 4471 Å line in air is reported as 4473 Å, the vacuum wavelength. The formula for conversion from between air and vacuum can be found in Morton (1991). Where ambiguities arise, the quantum numbers corresponding to a given wavelength can be obtained from Table 4.

Lines whose fluxes are thought to be uncertain to more than 5% due to the lack of collisional data from the 2^1S and 2^3S levels to levels with $n \geq 5$ are marked. See §3.1 for further discussion. The last four columns in Tables 5-7 contain a fit to the emission coefficients of the form $4\pi j_{line}/n_e n_{He+} = a_j t^{b_j} e^{c_j/t}$, where the maximum percentage difference between the fitting function and the calculated results is e_j . A grid with an extended density and temperature range, finer resolution, and more transitions, is available from the authors.

3.1. Collisional effects

In estimating helium abundances it has become standard to use the recombination cascade calculations of Brocklehurst (1972) or S96 and apply a correction for collisional enhancement of these lines. Since all of the rates out of the 2^3S level are low, substantial populations can build up in this level, and collisional transitions from 2^3S to upper levels are significant. KF95 have most recently estimated these effects using the same atomic data set as this calculation. In Table 8, we compare our calculated population fraction in the 2^3S levels with those derived by KF95, where they used the formula

$$\frac{n(2^3S)}{n_{He+}} = \frac{n_e \alpha_B^3}{A_{21} + n_e q_{tot}}, \quad (6)$$

where α_B^3 is the case B recombination into the triplet levels, A_{21} is the spontaneous decay rate to 1^1S and q_{tot} is the sum of all collisional transition rates (both excitation and ionization) from 2^3S into the singlet ladder. We show cases for $t = 2$ since higher temperatures give larger Boltzmann factors, emphasizing the collisional enhancement.

For the low density regime, $n_e \leq 10^2 \text{ cm}^{-3}$, where $A_{21} n_e q_{tot}$, our calculated 2^3S population is systematically 3.3% higher than that of KF95. This is completely attributable to the difference in the case

B triplet recombination rate, α_B^3 . KF95 used a fit to the recombination rate of Osterbrock (1989) which underestimated this rate by 3.3%. Although S96 did not report the total recombination rate, his value matched that of Brocklehurst (1972) nearly exactly.

For higher densities, where the collisional term becomes important, the remaining differences are due to two factors: First, KF95 use a power-law fit to the collisional rate, $q_{tot} = 3.61 \times 10^{-8} t^{0.5}$, which differs from our value by only 1% at $t = 1$, but exceeds our rate by 40 % at $t = 0.5$ and 19% at $t = 2$. This leads KF95 to underestimate the 2^3S population. However, these differences do not translate directly into emissivity differences. Second, as the densities increase, a non-negligible population builds up in the 2^1S level, and electrons are transferred back from the singlet into the triplet ladder. For $t = 1$, this effect increases the 2^3S population from what one calculates using the above equation by 6% for $n_e = 10^6 \text{ cm}^{-3}$ and 94% for $n_e = 10^8 \text{ cm}^{-3}$. In high density environments, therefore, it is necessary to calculate the singlet and triplet ladders simultaneously, as emphasized by AN89.

Table 8 also shows our calculation for the ratio of collisional-to-recombination contributions for selected emission lines and a comparison to the values calculated from KF95. Apart from propagating the differences for $n(2^3S)$, the remaining differences are due to the fact that KF95 included collisional excitation to $n = 5$ for selected lines. For emission lines originating from $n_u \leq 4$, this contribution is less than 5%, for $n_e \leq 10^6 \text{ cm}^{-3}$, but for lines from $n_u = 5$, such as 4026 Å or 4387 Å, the effect is obviously important.

We have decided not to include collisional rates to $n = 5$ from the unpublished results of SB93 as they are not converged. However, we have identified the lines with $j/j_{4471} > 10^{-2}$ for which our predictions would change significantly, by assuming that the collision strength to each $n = 5$ level is 50% of that to the corresponding $n = 4$ level. For low densities ($n_e = 10^2 \text{ cm}^{-3}$), the intensity of all but one emission line with $n_u = 5$ increase by less than 3%; lines with $n_u \leq 4$ increase by less than 0.4%.

For a density of $n_e = 10^6 \text{ cm}^{-3}$ and $t = 2.0$, lines with $n_u = 5$ increase by up to 70% from the tabulated predictions, except for 4122Å which is enhanced by a factor of 2.5. Several bright lines are also enhanced by a few percent from the values in Table 7 : 6678 Å(1.0%), 5876 Å(4.8%), 4471 (3.9%). Thus, unless one is interested in lines with $n_u = 5$, or wishes to obtain accuracies of better than 5% for bright lines in nebulae with $n_e > 10^6 \text{ cm}^{-3}$, the calculations presented here should be sufficiently accurate.

Which collisional rates matter? We explored the effect of turning off all collisional rates except for those with $\Delta n = 0$ and transitions from $2^1 S$ and $2^3 S$. We found a difference of at most 0.5% for lines with $j/j_{4471} > 10^{-2}$ over the temperature range $t = 0.5 - 2$ and density range $n_e = 10^0 - 10^8 \text{ cm}^{-3}$. Thus for this range of temperature and density, all other collisional transitions may be safely ignored.

3.2. Primordial helium abundance and uncertainties

The calculations presented here provide a grid of emission coefficients as a function of density and temperature. Assuming that optical depth effects are negligible, ionization correction factors are accounted for, and given a temperature and density from other spectral diagnostics, these calculations may be combined with observed line fluxes to estimate the nebular helium abundance of an object. The fitting functions given in Table 5-7 should be sufficiently accurate for most applications, however for cosmological studies, we present even more accurate fits here together with a detailed treatment of the uncertainties.

In order to simplify our fitting function, we consider a restricted range of temperatures and densities

appropriate for low metallicity extragalactic H II regions: $2 > t > 1.2$ and $300 > n_e > 1 \text{ cm}^{-3}$. We also consider the brightest optical lines which are not likely to be severely affected by collisional or radiative transfer effects: for singly ionized helium these are 4471 Å, 5876 Å, 6678 Å, and for doubly ionized helium, 4686 Å.

If the ratio of the observed helium line intensity to the $H\beta$ intensity is given by $r_{line} = I_{line}/I_{H\beta}$, then the helium abundance by number using a given line is

$$y_{line} = r_{line} f_{line}(n_e, t), \quad (7)$$

where the abundance by number can be converted to helium mass fraction using the relationship of Pagel et al. (1992),

$$Y = \frac{4y[1 - 20(O/H)]}{1 + 4y}, \quad (8)$$

and $y = ICF \times (y^+ + y^{++})$ is the ionization correction factor (see Pagel et al 1992) times the sum of y^+ , the singly ionized helium fraction determined using the He I lines, and y^{++} , the doubly ionized helium fraction determined using He II 4686.

The function $f(n_e, T)$ comes from combining our calculations with the $H\beta$ emissivities of Storey & Hummer (1995). We have determined a fitting function for $f(n_e, T)$ for the He I and He II emission lines of the form $f = At^B$, where $B = B_0 + B_1 n_e$. The parameters and goodness of fit statistics are given in Table 9. The fitting function is accurate to within 1% over the entire temperature/density interval.

As emphasized by Olive, Skillman, & Steigman (1997a,b), if the calculated helium emissivities are used to derive accurate helium abundances, it is important to make detailed estimates for systematic sources of uncertainty. Therefore, we need to assess the sources of error in the helium fraction

$$\sigma_y = \sqrt{\sigma_f^2 r^2 + \sigma_r^2 f^2} \quad (9)$$

where σ_r is the observational uncertainty. The analysis uncertainty, σ_f , arises from three sources which we add in quadrature: (1) uncertainties introduced by the fact that we use a fitting function rather than the exact tabulated emissivities, (2) uncertainties due to uncertainties in the atomic data, (3) uncertainties derived from uncertainties in the input density and temperature. This can be written as

$$\sigma_f^2 = \sigma_{fit}^2 + \sigma_{atomic}^2 + \sigma_n^2 \left(\frac{\partial f}{\partial n_e} \right) + \sigma_t^2 \left(\frac{\partial f}{\partial t} \right), \quad (10)$$

where σ_n and σ_t are the uncertainties in the electron density and normalized temperature, and the partial derivatives are $\partial f/\partial t = ABt^{B-1}$ and $\partial f/\partial n_e = AB_1(\ln t)t^B$. In the cases where there is a significant slope with density and large uncertainties on n_e , it is recommended that the uncertainty be determined by calculating the value of f over a range of densities, rather than using $\partial f/\partial n$.

Strictly speaking, use of a fitting function introduces a systematic rather than random uncertainty into our estimate. Table 9 both the maximum absolute value of deviation over the fitting region as well as the standard deviation so that one can limit the systematic uncertainty.

Characterizing the uncertainties in all the atomic data that are incorporated in this calculation is a difficult task. This is principally because errors in the atomic data will almost certainly be systematic rather than random, since the majority of data come from numerical calculations which will have built-in approximations and assumptions. As a result, calculated atomic data are rarely reported with uncertainty estimates. Therefore, attempts to calculate the uncertainty for an emission line intensity are somewhat subjective and the error estimates given here should be considered illustrative rather than definitive. Nevertheless, given the importance of identifying and characterizing all the sources of uncertainty in determination of primordial helium abundances, we have made such an attempt.

For the restricted range of temperature and density in §3.2, we did a set of calculations where for each run we randomly adjust each atomic parameter each time, using the uncertainty estimates given in the appendix. The revised atomic parameter is assumed to be Gaussian distributed about the given value with a standard deviation given by the percentage confidence levels given in the previous sections. After 1000 runs, we find that the mean line fluxes and standard deviations are sufficiently converged. There is no significant skewness in the resulting distribution. We then average the fractional standard deviation over the range of density and temperature considered. For the lines of interest, we find σ_{atomic}/f is in the range 1.3-1.5%. The greatest source of uncertainty at the current time is the recombination rates to individual levels. These rates consist of a patchwork of different approximations for different levels and temperatures. A coherent treatment of these rates should be quite valuable.

To illustrate the use of these uncertainties, we consider the case of the low metallicity galaxy I Zw 18 using the data of Izotov & Thuan (1998). For the SE knot, they have determined $r_{6678} = 0.0267 \pm 0.0010$ and $r_{4686} = 0.0076 \pm 0.0009$. The [O III] determined temperature is $t = 1.88 \pm 0.04$ and the density from [S II] is $n_e = 10 \text{ cm}^{-3}$. Using the fitting function data from Table 9, we find $y^+ = y_{6678} = 0.0807$ $y^{++} = y_{4686} = 6.80 \times 10^{-4}$. This agrees with the estimates of Izotov & Thuan (1998), since they also used the atomic data of S96, and the measured densities are sufficiently low that collisional corrections are unnecessary.

If we assume that the uncertainty in density is $\sigma_n = 10 \text{ cm}^{-3}$, then the contributions to the flux ratio uncertainty σ_f^2 are $\sigma_{fit} = 3.05 \times 10^{-3}$, $\sigma_t(\partial f/\partial t) = 0.016$, $\sigma_n(\partial f/\partial n) = 3.82 \times 10^{-3}$, and $\sigma_{atomic} = 0.039$, so that it is the atomic data uncertainty that dominates this part of the error budget, followed by the temperature. The uncertainty in y arising from the analysis is therefore $\sigma_f = 0.042$. In this case, it is the measurement uncertainties that dominate the uncertainty in y , since $\sigma_{fr} \ll \sigma_r f$. For both source of uncertainty to be equal, σ_f would have to be 0.113 rather than the calculated 0.042.

In this example, a density uncertainty of 10 cm^{-3} is unrealistically small. If the density uncertainties are sufficiently large, it is necessary to use calculate the value of f over the possible density range, rather than using $\sigma_n(\partial f/\partial n)$. Using a density range of $100 > n > 0 \text{ cm}^{-3}$, we find that f varies by $\Delta f = 0.034$, a significantly larger uncertainty than $\sigma_n(\partial f/\partial n) = 3.82 \times 10^{-3}$.

Frequently helium abundance are calculated by weighting the results from different lines by the respective uncertainties. This gives the greatest weight to the brightest line measured, usually 5876 Å. In the future, the analysis uncertainties characterized here should also be included when doing this final weighting.

4. Comparison to data and future work

An ideal recombination model should be able to match all of the observed helium emission line intensities simultaneously. Any differences between the predictions and the observed line fluxes will indicate either errors in the calculations or incompleteness in the assumptions of our model. In Figure 2, we plot the ratio of observed helium emission line intensities to predictions for three nebulae: NGC 1976 in Orion (Osterbrock et al. 1992), NGC 6572, and IC 4997 (Hyung, Aller & Feibelman 1994a,b). The predicted emission lines are calculated using $(n_e, T_e) = (4000 \text{ cm}^{-3}, 9000 \text{ K})$ for NGC 1976, $(10^4 \text{ cm}^{-3}, 11000 \text{ K})$ for NGC 6572, and $(10^6 \text{ cm}^{-3}, 10800 \text{ K})$ for IC 4997. Figures 2a and 2b show the ratio of observed-to-predicted lines ratios before and after correcting for collisional excitation. Note that the ratio of observed-to-predicted flux for 4471 is one by definition. As expected the inclusion of collisional effects results in better agreement for the $n^3S - 2^3P$ series of lines (7065 Å, 4713 Å, etc) which are most sensitive to collision excitation out of 2^3S . The 7065/4471 ratio decreases from four to 1.8 times the predicted ratio. Of course, the third ratio in this series, 4121/4471 Å, gets slightly worse. Our collision corrected lines agree well with those estimated by Kingdon & Ferland (1996) which can be obtained by dividing the first column by the second column tabulated for each object in their Table 1.

After the collisional corrections have been applied, the most discrepant bright optical lines are from the dense planetary nebula IC 4997: the ratios 7281/4471 and 6678/4471 are both less than predicted. The origin of this discrepancy is not clear, but since the discrepancy is monotonic with wavelength, Kingdon & Ferland (1996) have suggested that it is due to internal extinction associated with an unusually high gas-to-dust ratio in this object.

Unfortunately, the observations to which we are comparing our calculations had no error estimates for line fluxes; in order to weight the significance of individual lines, we vary the point size according to the measured brightness of the lines. Figure 2 shows that the the infrared transitions to $n = 3$ show roughly a factor of three scatter evenly distributed about the predicted value. This scatter may be due to measurement error, since these lines are faint and suffer from uncertain telluric absorption. Without error estimates though, it is hard to be sure that this is the entire explanation.

Finally, for the UV lines shortward of 4000 Å, it appears that the UV lines are systematically high. In particular, there appears to be some curvature of the ratio upward as the wavelength of the line decreases from 3614 Å to 3354 Å. It seems likely that this is also due to radiative transfer effects. Using HST spectra, Martin et al (1996) have seen a similar effect, rule out extinction as a possibility and suggest that radiative transfer effects are present.

Over the last four years, high resolution optical spectra, containing several helium lines each, and estimates of physical conditions have been obtained for over a dozen planetary nebulae by Hyung, Aller, & Feibelman (see Hyung & Aller 1997 and references therein). We only compare to two of those nebulae here, but clearly there is now a large data base with which to compare our helium emissivity calculations. Such a data base will be extremely useful to see if deviations from our predictions correlate with physical properties of the nebulae. A more detailed comparison of our calculations to this expanded database will be given in future work.

What can be done to further improve the reliability of predictions for helium emission lines? There are several areas where the atomic model needs improvement or verification. First, the recombination rates used are a patchwork of rates from different sources, and are probably the single largest source of uncertainties in the resulting emission line intensities. Second, as discussed by S96, strong singlet-triplet mixing can occur for high l states. And finally, an independent evaluation of the collisional rates for high n states would be valuable, particularly as we found discrepancies as high as a factor of seven in collisional

rates using the Seaton (1962) impact parameter method and the **R**-matrix calculations of SB93.

Finally, in order to compare with observational measurements of helium line intensities it is necessary to include radiative transfer effects to determine what effects this has on the resulting line ratios. All of our results presented here are in the limit of Case B, in which all permitted transitions to 1^1S are thought to be immediately reabsorbed, and all other transitions are optically thin. Both nebulae with sufficiently low optical depth in transitions to 1^1S and nebulae with sufficiently high optical depth in 2^3S will depart from this assumption. The standard reference for radiative transfer are those of Robbins (1968) and Robbins & Bernat (1973). Recent examinations of this issue are given by AN89, and also by Proga, Mikolajewska, & Kenyon (1994) and Sasselov & Goldwirth (1995) who took their data from AN89. Given the improvements in the atomic data afforded by the re-examination of A-values (Kono & Hattori 1984), the recombination rates (S96), and collisional rates (SB93), a re-examination of radiative transfer issues should be very useful. This will be the subject of future work.

ACKNOWLEDGEMENTS: We would like to acknowledge useful conversations with Phil Stancil concerning the effect of charge transfer on affecting the population of the 2^3S level, and Jim Kingdon and Hagai Netzer for supplying codes, advice, and calculations, as well as for numerous useful comments on this manuscript. We are also grateful for support from the Minnesota Supercomputer Institute and NASA LTSARP grant no NAGW-3189.

APPENDIX

A. Atomic data

The reliability of the calculations presented here is determined by the accuracy of the input atomic data. In Tables 1-4, we give a small subset of the atomic data for future researchers to compare with. Here, we summarize the techniques and references for the rest of the input data.

A.1. Energy levels (E)

$l \leq 2$: When available, the energy levels from the compilation of Martin (1973) were used. For levels above those given by Martin, n_{top} , energy levels were calculated by extrapolating the quantum defect of these lower levels, $d = n - n^*$, where n^* is the effective quantum number. The last value of n for which a term value is given, and the adopted quantum defects are given in Table 10.

$l \geq 3$: Hydrogenic energy levels were assumed, i.e. $E = -E_o/n^2$, where $E_o = 13.60577 \text{ eV}$.

All energy levels should be accurate to within 0.5%, and are given in Table 1. Wavelengths are calculated from these energy levels. In the tables, we use these vacuum wavelengths. In the text, we refer to transitions using the standard wavelengths in air.

A.2. Spontaneous radiative transitions (A)

$n_u \leq 9$: Using values of Kono & Hattori (1984).

$n_u \geq 10$ and $n_l \leq 6$: Using Coulomb approximation (see Smits 1991a), but each series of transitions to n_l has been scaled to match the Kono & Hattori (1984) values for transitions from $n_u = 9$ to n_l .

$n_u \geq 10$ and $n_l \geq 7$: Using Coulomb approximations as in Smits (1991a).

Non-permitted transitions: Rates for the transition from 2^3S to 1^1S is from Hata & Grant (1981), 2^3P to 1^1S from Lin, Johnson, & Dalgarno (1977) and the two-photon transition from 2^1S to 1^1S is from Drake (1979). The remaining forbidden transitions among the $n = 2$ levels are taken from Mendoza (1983).

Nearly all previous calculations of helium emission lines before Smits used A values taken from the compilation of Wiese, Smith, & Glennon (1966). Many of these values derived from the calculations of Dalgarno & Kingston (1958). There are numerous cases, such as the 3187 Å line, in which the A-values differ by more than 10%. Therefore, if accuracies of a few percent or better are desired, these new calculations should be used. Kono & Hattori (1984) estimate all values are accurate to within 1%, and many to better than 0.1%. Here we adopt an uncertainty of 1% for all lines.

A.3. Radiative recombination rates (α)

1S , 3S $n \leq 10$; 1P , 1D , 3D $n \leq 9$; 3P $n = 2, 3$: Recombination rates obtained by detailed balance from He I photoionization cross sections of Fernley et al. (1987) using integration scheme outlined by Burgess (1965) and Brocklehurst (1971). Tabulated values of the photoionization cross-sections σ and energies ω were obtained from TOPbase (Cunto et al. 1993), and the necessary grid of points needed for the integration was obtained by linearly interpolating $\log \sigma$ vs $\log \omega$. Method described in S96.

3P $n = 4$ to 12, 1P $n = 10, 11, 12$: Quantum defect method was used: for $T < 2500$ K algorithm of Burgess & Seaton (1960a) and for $T \geq 2500$ K algorithm of Peach (1967)

Remaining levels: Scaled hydrogenic rates used for large n . Scaling factor was determined from ratio of TOPbase to hydrogen recombination rate at $n = 10$ for S levels and $n = 9$ for D levels. For the P series with $n > 12$ scaled hydrogenic rates were used, scaling factor taken from quantum defect method results at $n = 12$. Hydrogenic rates are described in S91.

There have been several works that examine the total photoionization cross section as a function of energy. Opacity Project calculations (Fernley et al 1987; Cunto et al 1993) used to derive the photoionization cross section have been compared with observational data from threshold to 120 eV showing differences of less than 1% (Samson et al. 1994). Samson et al. then critically evaluate the available literature to extend the cross sections to 8 keV. Yan et al (1998) have performed theoretical calculations at these higher energies, and suggested revision in the Samson et al cross section.

In comparing calculations of cross-section to individual levels at the threshold energies, Hummer & Storey (1998) found that the Fernley et al. (1987) calculations agreed to within 1% with results expected using the oscillator strengths of Drake (1996). However, much larger differences than this were found for the 1^1S series, which motivated Hummer & Storey (1998) to perform ab initio calculations so as to provide more reliable cross-sections for the individual levels. Although the resulting individual recombination rates are not yet available, we can compare the total recombination rate here with the values from Hummer & Storey (1998). At $T = 10^4$ K, their value for α_B^1 and α_B^3 are 1.3% and 1.1% higher than our values.

In our calculations, we estimate that uncertainties in the individual rates are probably of order 2%. This uncertainty can eventually be reduced by using the new Hummer & Storey rates which would eliminate the heterogeneous treatment of individual rates.

A.4. Collision strengths (Ω)

$\Delta S \neq 0$ and $n_u \geq 5$: No collisional coupling between the singlet and triplet state is considered for $n_u \geq 5$.

$\Delta S \neq 0$ and $n_u \leq 4$: Coupling between all triplet and singlet levels for $n_u \leq 4$ due to electron collisions only is taken from SB93, by linearly interpolating Ω from their Table II. For temperatures below the minimum calculated by SB93, $\Omega = 0$; for temperatures above the maximum temperature, T_{max} , $\Omega = \Omega(T_{max})$. This is done to minimize the effects of uncertain extrapolation.

$\Delta n \neq 0$, and $n_u \geq 5$: Only electronic transitions are considered. Hydrogenic collision rates are used for $l \geq 3$; impact-parameter treatment of Seaton (1962) is used for $l \leq 2$.

$\Delta n \neq 0$ and $n_u \leq 4$: Only electronic transitions are included and are taken from SB93.

$\Delta n = 0$ and $n \geq 2$: Transitions involving electrons, protons, and ionized helium atoms are included, assuming $n_e = n_p = 10n_{He^+}$. Although this assumption technically makes the emission lines predictions dependent on chemical abundance and ionization state, the dependence is normally so weak as to be negligible. For a given n , the low l values are calculated using the impact parameter method of Seaton (1962); when a value of l is reached such that the computationally faster method of Pengelly & Seaton (1964) matches the Seaton (1962) method within 6%, the second method is used for all higher l states. We do not use SB93 rates since only a few of these rates at low temperature are judged by them to be converged.

$\Delta n = 0$ and $n = 2$: We use the electron collision rates of SB93, and the method of Seaton (1962) for the proton and helium atom collisions. The energy difference is large enough that electron collisions completely dominate the total.

Table 4 contains the collision strengths used for a range of temperature together with power-law fits. These collision strengths may be converted to collisional rates using the standard formula in Osterbrock (1989, p. 55). Note, however, that many of the rates of SB93 are not monotonic with temperature, since they integrate a Maxwellian distribution of electron velocities over a cross-section with resonances. As a result, any attempt to fit these rates with simple power laws (as in Clegg 1987 or Kingdon & Ferland 1996) will necessarily result in a loss of accuracy. Whether this loss of accuracy is significant depends upon the relative importance of collisional processes in determining the line of interest. It is also worth noting that in the process of comparing $\Delta n \neq 0$ collisional rates using Seaton impact parameter method (1962) to the more accurate values of SB93, we found differences of up to a factor of seven in the electron impact collision strengths. However, there were not enough transitions in common for the two data sets to search for systematic effects with quantum number. For the collision strengths of SB93, we assume an uncertainty of 2%. For all other collision strengths, we assume a very optimistic 20%.

A.5. Collisional ionization (C^{ion})

Following AN89, we use the collisional ionization rate of Taylor, Kingston & Bell (1979) for the 2^3S level, and scaled hydrogenic rates of Vriens & Smeets (1980) for all other rates. Collisional ionization becomes most significant at high densities for high n levels; however, the calculations of S96 which are used to calculate the effect of upper levels on the recombination cascade do not currently include collisional ionization. Fits to the collisional rates of the form $C^{ion} = a_C t^{b_C} e^{C_C/t}$ are given in Table 2.

A.6. Three-body recombination (α^{tbr})

Three-body recombination is calculated using detailed balance from the above rates, fit as $\alpha^{tbr} = \alpha_4^{tbr} t^{b_{\alpha^{tbr}}}$ and given in Table 2.

A.7. Other possible rates

There are several other possible physical effects that could be considered here, but are not included in this work.

Charge transfer: Clegg (1987) has discussed the possibility that charge transfer could be important in affecting the 2^3S population. For reactions of the form $X + He(2^3S) \rightarrow$ products, he is able to rule out the importance of this transition if X is a metal, and standard nebular abundances are assumed. (For a case in which this assumption breaks down see models of H-poor supernova ejecta by Swartz 1994.) Using the rates for proton collisions of Janev et al. (1987), Baldwin et al. (1991) also shows that proton collision exchange is also negligible.

Photoionization from metastable levels: Clegg & Harrington (1989) have also considered the effects of photoionization from the metastable 2^3S level. This effect can be considerable in optically-thick planetary nebulae, but is found to be negligible for optically-thin planetaries and low density H II regions. We neglect these effects here as it requires detailed modelling of the nebular spectrum.

Dielectronic recombination: At sufficiently high temperatures, $T > 50,000 K$, dielectronic recombination starts to become important relative to radiative recombination (Burgess 1964). The excitation of the helium atom to an autoionizing state will change the energy level structure and the resulting cascade. This complication is not addressed in this paper, but is considered in Bhatia & Underhill (1986).

Radiative absorption: A final effect which has been found to be important (Robbins 1968, Robbins & Bernat 1973) is the absorption of line photons from the ground state 1^1S and the metastable levels 2^1S and 2^3S . In this work, we assume that all line photons associated with decays to 1^1S are reabsorbed on the spot (Case B). Treatment of absorption of line photons from the 2^1S and 2^3S levels is deferred to later work.

REFERENCES

Almog, Y. & Netzer, H. 1989, MNRAS, 238, 57 (AN89)

- Baldwin, J.A. et al. 1991, *ApJ*, 374, 580
- Berrington, K.B., Burke, P.G., Freitas, L.C.G. & Kingston, A.E. 1985, *J Phys B*, 18, 4135
- Berrington, K.B. & Kingston, A.E. 1987, *J Phys B*, 20, 6631
- Brocklehurst, M. 1971, *MNRAS*, 153, 471
- Brocklehurst, M. 1972, *MNRAS*, 157, 211
- Burgess, A. 1964, *ApJ*, 139, 776
- Burgess, A. 1965, *Mem. R. Astronom. Soc.*, 69, 1
- Burgess, A. & Seaton, M.J. 1960a, *MNRAS*, 120, 121
- Clegg, R.E.S. 1987, *MNRAS*, 229, 31P
- Clegg, R.E.S. & Harrington, J.P. 1989, *MNRAS*, 239, 869
- Cota, S.A. 1987, PhD Thesis, Ohio State University
- Cox, D.P. & Daltabuit, E. 1971, *ApJ*, 167, 257
- Cunto, W., Mendoza, C., Ochsenbein, F., Zeippen, C. J., 1993, *A&A*, 275, L5
- Dalgarno, A. & Kingston, A.E., 1958, *Proc. Phys. Soc. London A*, 70, 802
- Drake, G.W.F. 1979, *Phys. Rev A*, 19, 1387
- Ferland, G.J. 1986, *ApJ*, 31, L67
- Fernley, J. A., Taylor K. T., Seaton M. J. 1987, *J. Phys. B Atom. Molec. Phys*, 20, 6457
- Hata, J. & Grant, I.P. 1981, *J Phys B*, 14, 2111
- Hyung, S. & Aller, L.H. 1997, *MNRAS*, 292, 71
- Hyung, S., Aller, L.H., and Feibelman, W.A. 1994a, *MNRAS*, 269, 975
- Hyung, S., Aller, L.H., and Feibelman, W.A. 1994b, *ApJS*, 93, 465
- Izotov, Y.I. & Thuan, T. X. 1998, *ApJ*, in press
- Janev, R.K., Langer, W.D., Post, D.E., & Evans, K. 1987. *Elementary Processes in Hydrogen-Helium Plasmas* (Berlin: Springer)
- Kingdon, J. & Ferland, G.J. 1995, *ApJ*, 442, 714 (KF95)
- Kingdon, J. & Ferland, G.J. 1996, *MNRAS*, 282, 723
- Kono, A. & Hattori, S. 1984, *Phys Rev A*, 29, 2981
- Lin, C.D., Johnson, W.R., and Dalgarno, A. 1977, *Phys Rev A*, 15, 154
- Lockyer, J.N. 1868, *Proc. R. Soc.*, 17, 131
- Martin, W.C. 1973, *J. Phys. Chem. Ref. Data*, 2, 257
- Martin, P.G. et al. 1996, *BAAS* 189, #106.01
- Mathis, J. 1957, *ApJ*, 125, 318
- Mendoza, C. 1983, in *IAU Symp. 103, Planetary Nebulae*, ed. D. Flower (Dordrecht: Reidel), 245
- Morton, D.C. 1991, *ApJS*, 77, 119
- Olive, K.A., Skillman, E.D., and Steigman, G. 1997a, *ApJ*, 483,788
- Olive, K.A., Skillman, E.D., and Steigman, G. 1997b, *ApJ* 489, 1006

- Osterbrock, D.E. 1989, *Astrophysics of Gaseous Nebulae and Active Galactic Nuclei* (Mill Valley: University Science Books)
- Osterbrock, D.E., Tran, H.D., Veilleux, S., 1992, *ApJ*, 389, 305
- Pagel, B.E.J., Simonson, E.A., Terlevich, R.J., & Edmunds, M.G. 1992, *MNRAS*, 255, 325
- Peach, G. 1967, *Mem. Roy. Astr. Soc.*, 71, 13
- Peimbert, M. & Torres-Peimbert, S. 1974, *ApJ*, 193, 327
- Pengelly, R.M. & Seaton, M.J. 1964, *MNRAS*, 127, 165
- Press, W.H., Flanner, B.P., Teukolsky, S.A., and Vetterling, W.T. 1986, *Numerical Recipes: The Art of Scientific Computing* (New York: Cambridge University Press).
- Proga, D., Mikolajewska, J., & Kenyon, S.J. 1994, *MNRAS*, 268, 213
- Robbins, R.R. 1968, *ApJ*, 151, 497
- Robbins, R.R. & Bernat, A.P. 1973, *Mem. Soc. Roy. Sci. Liege*, 6 (5), 263
- Robbins, R.R. & Robinson, E.L. 1971, *ApJ*, 167, 249
- Sasselov, D. & Goldwirth, D. 1995, *ApJL*, 444, 5
- Sawey, P.M.J. & Berrington, K.A. 1993, *Atomic Data Nucl. Data Tables*, 55, 81 (SB93)
- Seaton, M.J. 1962, *Proc. Phys. Soc.*, 79, 1105
- Skillman, E.D., Terlevich, R.J., Kennicutt, R.C., Garnett, D.R., & Terlevich, E. 1994, *ApJ*, 431, 172
- Smits, D.P. 1991a, *MNRAS*, 248, 193
- Smits, D.P. 1991b, *MNRAS*, 251, 316
- Smits, D.P. 1996, *MNRAS*, 278, 683 (S96)
- Storey, P.J. & Hummer, D.G. 1995, *MNRAS*, 272, 41
- Swartz, D.A. 1994, *ApJ*, 428, 267
- Taylor, I.R., Kingston, A.E., & Bell, K.L. 1979, *J. Phys. B.*, 12, 3093
- Vriens, L. & Smeets, A.H.M. 1980, *Phys. Rev. A*, 22, 940.
- Walker, T.P., Steigman, G., Schramm, D.N., Olive, K.A., & Kang, H. 1991, *ApJ*, 376, 51
- Wiese, W.L., Smith, M.W., & Glennon, B.M. 1966, *Atomic Transition Probabilities: NSRDS-NBS 4(1)*

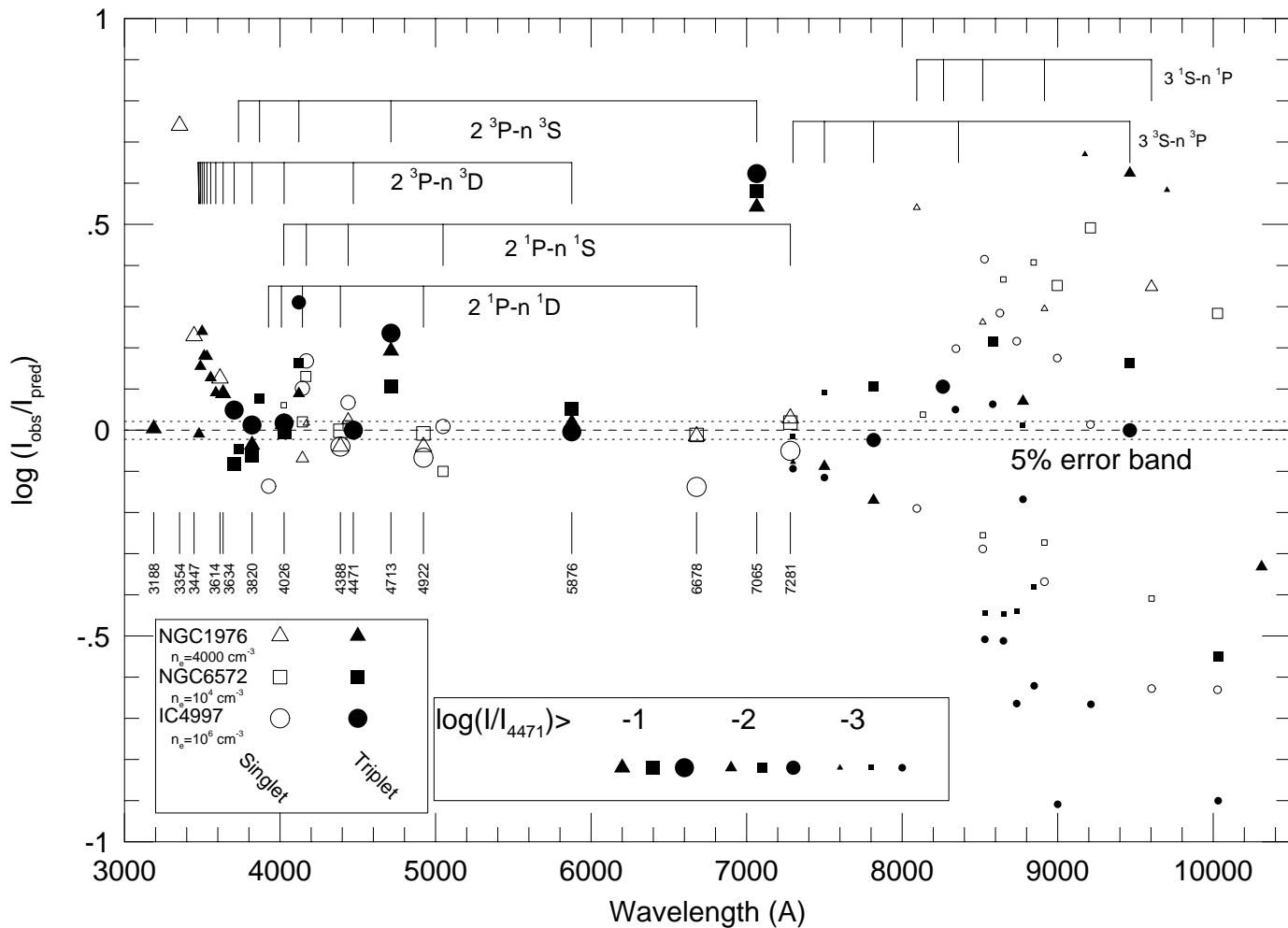


Fig. 2a.— Comparison between theoretical emissivities (without collisional corrections) and observed helium emission line intensities for three nebulae: Orion (NGC 1976) with $n_e = 4000 \text{ cm}^{-3}$ and $T_e = 9,000 \text{ K}$, and the planetaries NGC 6572 ($n_e = 10^4 \text{ cm}^{-3}, T_e = 11,000 \text{ K}$) and IC4997 ($n_e = 10^6 \text{ cm}^{-3}, T_e = 10,800 \text{ K}$). Singlet and triplet lines are shown with open and filled symbols respectively. All lines have been normalized to 4471 \AA , and where the symbol size indicates the brightness of the lines. Selected “families” of lines are

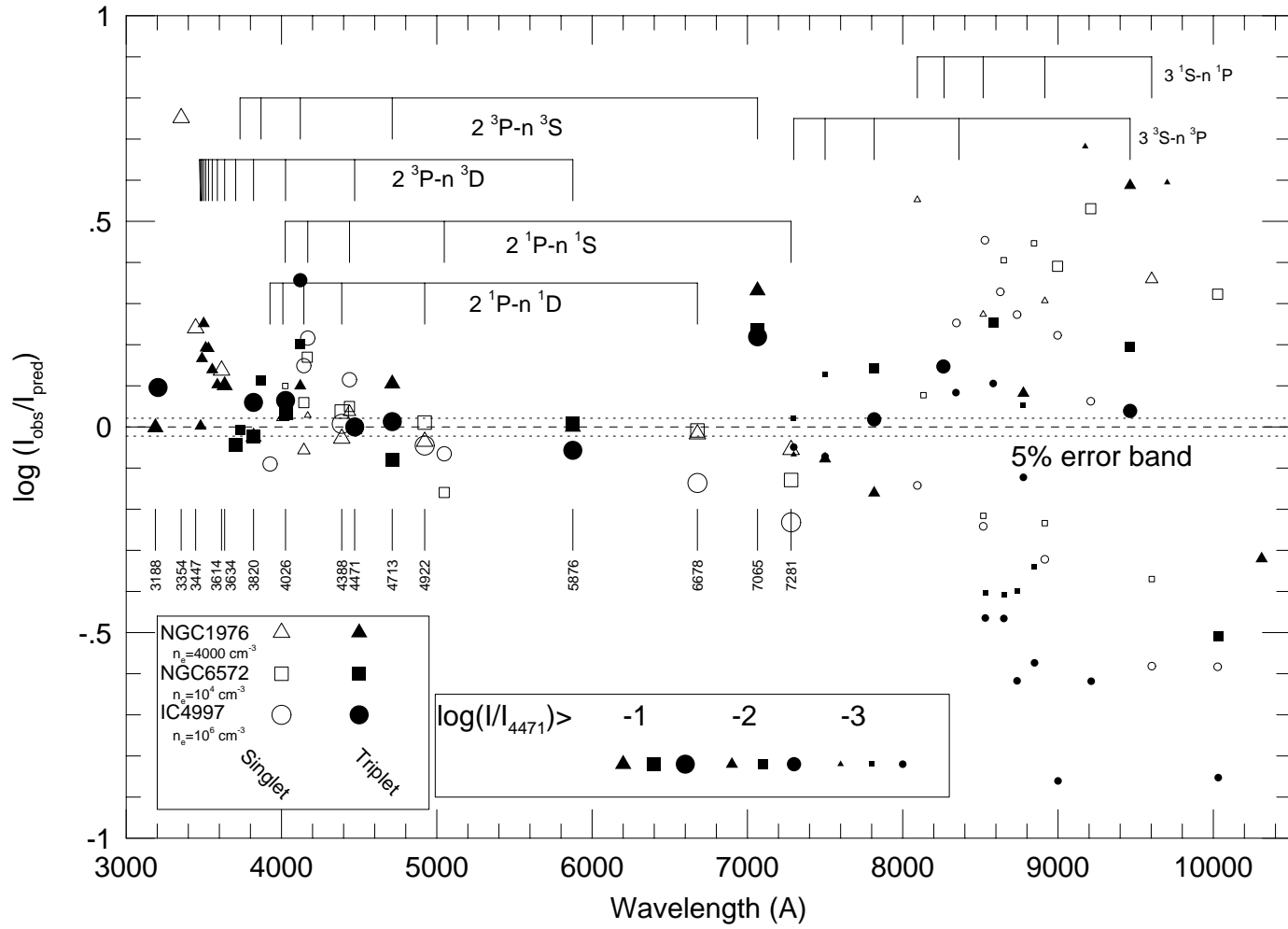


Fig. 2b.— Same as Figure 2a, but after collision excitation from 2^3S and 2^1S have been included

Table 1. Recombination data for individual levels of He I

n	l	g_S	E_{nls} (eV)	α_4 ($\text{cm}^3 \text{s}^{-1}$)	b_α	e_α
	α_A^{tot}			4.27×10^{-13}	-0.678	$\pm 0.00\%$
	α_B^{tot}			2.72×10^{-13}	-0.789	$\pm 0.01\%$
	α_B^1			6.23×10^{-14}	-0.827	$\pm 0.02\%$
1	0	1	-24.5876	1.54×10^{-13}	-0.486	$\pm 0.27\%$
2	0	1	-3.9716	5.55×10^{-15}	-0.451	$\pm 0.34\%$
2	1	1	-3.3694	1.26×10^{-14}	-0.695	$\pm 3.36\%$
3	0	1	-1.6671	1.62×10^{-15}	-0.444	$\pm 0.23\%$
3	1	1	-1.5005	5.01×10^{-15}	-0.700	$\pm 3.34\%$
3	2	1	-1.5134	4.31×10^{-15}	-0.872	$\pm 4.77\%$
4	0	1	-0.9139	7.00×10^{-16}	-0.445	$\pm 0.08\%$
4	1	1	-0.8453	2.43×10^{-15}	-0.708	$\pm 3.39\%$
4	2	1	-0.8510	2.67×10^{-15}	-0.871	$\pm 4.80\%$
4	3	1	-0.8504	1.38×10^{-15}	-1.046	$\pm 5.25\%$
5	0	1	-0.5762	3.66×10^{-16}	-0.454	$\pm 0.23\%$
5	1	1	-0.5416	1.35×10^{-15}	-0.718	$\pm 3.42\%$
5	2	1	-0.5447	1.60×10^{-15}	-0.873	$\pm 4.81\%$
5	3	1	-0.5442	1.22×10^{-15}	-1.048	$\pm 5.25\%$
5	4	1	-0.5442	4.46×10^{-16}	-1.183	$\pm 4.80\%$
	α_B^3			2.10×10^{-13}	-0.778	$\pm 0.01\%$
2	0	3	-4.7679	1.49×10^{-14}	-0.381	$\pm 1.41\%$
2	1	3	-3.6233	5.61×10^{-14}	-0.639	$\pm 2.45\%$
3	0	3	-1.8690	3.72×10^{-15}	-0.344	$\pm 1.38\%$
3	1	3	-1.5803	1.95×10^{-14}	-0.632	$\pm 2.41\%$
3	2	3	-1.5137	1.33×10^{-14}	-0.868	$\pm 4.72\%$
4	0	3	-0.9935	1.50×10^{-15}	-0.328	$\pm 0.90\%$
4	1	3	-0.8796	9.04×10^{-15}	-0.632	$\pm 2.47\%$
4	2	3	-0.8513	8.29×10^{-15}	-0.867	$\pm 4.74\%$
4	3	3	-0.8504	4.15×10^{-15}	-1.046	$\pm 5.25\%$
5	0	3	-0.6155	7.51×10^{-16}	-0.327	$\pm 0.57\%$
5	1	3	-0.5592	4.84×10^{-15}	-0.636	$\pm 2.47\%$
5	2	3	-0.5448	4.99×10^{-15}	-0.870	$\pm 4.75\%$
5	3	3	-0.5442	3.65×10^{-15}	-1.048	$\pm 5.25\%$
5	4	3	-0.5442	1.34×10^{-15}	-1.183	$\pm 4.80\%$

Note. — Radiative recombination rates and three-body recombination rate for individual levels can be determined by powerlaw fit $\alpha(t_4) = \alpha_4 t_4^b$. The maximum error of these fits over the temperature range $T = 5000 - 20000 \text{ K}$ is $\pm e_\alpha$. Calculations requiring higher accuracy or temperatures outside this range should contact authors for a grid of rates.

Table 2. Three body recombination and collisional ionization rates for He I

n	l	g_S	α_4^{tbr} ($\text{cm}^6 \text{s}^{-1}$)	$b_{\alpha^{tbr}}$	$e_{\alpha^{tbr}}$	$a_{C^{ion}}$ ($\text{cm}^3 \text{s}^{-1}$)	$b_{C^{ion}}$	$c_{C^{ion}}$	$e_{C^{ion}}$
1	0	1	3.18×10^{-31}	-0.905	$\pm 2.45\%$	3.36×10^{-9}	0.499	-28.625	$\pm 0.18\%$
2	0	1	1.21×10^{-29}	-1.117	$\pm 3.36\%$	1.33×10^{-7}	0.253	-4.733	$\pm 0.21\%$
2	1	1	4.96×10^{-29}	-1.138	$\pm 3.42\%$	1.81×10^{-7}	0.229	-4.037	$\pm 0.22\%$
3	0	1	5.94×10^{-29}	-1.236	$\pm 3.70\%$	6.58×10^{-7}	0.120	-2.072	$\pm 0.23\%$
3	1	1	2.14×10^{-28}	-1.252	$\pm 3.75\%$	7.93×10^{-7}	0.103	-1.880	$\pm 0.24\%$
3	2	1	3.52×10^{-28}	-1.251	$\pm 3.74\%$	7.81×10^{-7}	0.104	-1.895	$\pm 0.24\%$
4	0	1	1.67×10^{-28}	-1.326	$\pm 3.95\%$	1.87×10^{-6}	0.021	-1.207	$\pm 0.25\%$
4	1	1	5.72×10^{-28}	-1.338	$\pm 3.99\%$	2.13×10^{-6}	0.007	-1.128	$\pm 0.25\%$
4	2	1	9.42×10^{-28}	-1.337	$\pm 3.98\%$	2.11×10^{-6}	0.008	-1.135	$\pm 0.25\%$
4	3	1	1.32×10^{-27}	-1.338	$\pm 3.98\%$	2.11×10^{-6}	0.008	-1.134	$\pm 0.25\%$
5	0	1	3.57×10^{-28}	-1.399	$\pm 4.13\%$	4.02×10^{-6}	-0.059	-0.821	$\pm 0.25\%$
5	1	1	1.18×10^{-27}	-1.409	$\pm 4.15\%$	4.44×10^{-6}	-0.069	-0.781	$\pm 0.25\%$
5	2	1	1.95×10^{-27}	-1.408	$\pm 4.14\%$	4.40×10^{-6}	-0.068	-0.785	$\pm 0.25\%$
5	3	1	2.74×10^{-27}	-1.408	$\pm 4.15\%$	4.40×10^{-6}	-0.068	-0.784	$\pm 0.25\%$
5	4	1	3.52×10^{-27}	-1.408	$\pm 4.15\%$	4.40×10^{-6}	-0.068	-0.784	$\pm 0.25\%$
2	0	3	2.57×10^{-29}	-1.093	$\pm 3.29\%$	9.36×10^{-8}	0.280	-5.655	$\pm 0.21\%$
2	1	3	1.30×10^{-28}	-1.129	$\pm 3.40\%$	1.58×10^{-7}	0.240	-4.331	$\pm 0.21\%$
3	0	3	1.45×10^{-28}	-1.220	$\pm 3.66\%$	5.36×10^{-7}	0.138	-2.304	$\pm 0.23\%$
3	1	3	5.87×10^{-28}	-1.244	$\pm 3.73\%$	7.23×10^{-7}	0.111	-1.972	$\pm 0.23\%$
3	2	3	1.06×10^{-27}	-1.250	$\pm 3.74\%$	7.81×10^{-7}	0.104	-1.895	$\pm 0.24\%$
4	0	3	4.36×10^{-28}	-1.314	$\pm 3.92\%$	1.62×10^{-6}	0.035	-1.298	$\pm 0.25\%$
4	1	3	1.61×10^{-27}	-1.332	$\pm 3.97\%$	2.00×10^{-6}	0.014	-1.167	$\pm 0.25\%$
4	2	3	2.83×10^{-27}	-1.337	$\pm 3.98\%$	2.11×10^{-6}	0.008	-1.135	$\pm 0.25\%$
4	3	3	3.96×10^{-27}	-1.338	$\pm 3.98\%$	2.11×10^{-6}	0.008	-1.134	$\pm 0.25\%$
5	0	3	9.63×10^{-28}	-1.388	$\pm 4.11\%$	3.61×10^{-6}	-0.047	-0.866	$\pm 0.25\%$
5	1	3	3.37×10^{-27}	-1.404	$\pm 4.14\%$	4.21×10^{-6}	-0.064	-0.802	$\pm 0.25\%$
5	2	3	5.85×10^{-27}	-1.408	$\pm 4.14\%$	4.39×10^{-6}	-0.068	-0.785	$\pm 0.25\%$
5	3	3	8.21×10^{-27}	-1.408	$\pm 4.15\%$	4.40×10^{-6}	-0.068	-0.784	$\pm 0.25\%$
5	4	3	1.06×10^{-26}	-1.408	$\pm 4.15\%$	4.40×10^{-6}	-0.068	-0.784	$\pm 0.25\%$

Table 3. “Indirect”^a recombination rates for $n_{max} = 5$ (Case B)^b

n	l	g_S	α'_4 (cm^3s^{-1})	b'_α	$e_{\alpha'}(n_e = 10^2)^c$	$c_{\alpha'}$	$e_{\alpha'}(T_e = 10^4)^d$
2	0	1	2.25×10^{-15}	-0.766	$\pm 2.84\%$	0.000	$\pm 0.11\%$
2	1	1	3.11×10^{-15}	-0.879	$\pm 3.46\%$	0.008	$\pm 3.49\%$
3	0	1	6.09×10^{-16}	-0.782	$\pm 2.53\%$	0.000	$\pm 0.00\%$
3	1	1	1.30×10^{-15}	-0.876	$\pm 2.70\%$	0.008	$\pm 3.15\%$
3	2	1	2.64×10^{-15}	-1.114	$\pm 4.28\%$	0.003	$\pm 1.08\%$
4	0	1	2.44×10^{-16}	-0.783	$\pm 2.52\%$	0.000	$\pm 0.04\%$
4	1	1	6.50×10^{-16}	-0.854	$\pm 2.44\%$	0.008	$\pm 3.06\%$
4	2	1	1.64×10^{-15}	-1.106	$\pm 4.20\%$	0.003	$\pm 1.08\%$
4	3	1	2.31×10^{-15}	-1.271	$\pm 3.44\%$	-0.001	$\pm 0.15\%$
5	0	1	1.16×10^{-16}	-0.786	$\pm 2.47\%$	0.000	$\pm 0.11\%$
5	1	1	3.82×10^{-16}	-0.832	$\pm 2.15\%$	0.008	$\pm 2.93\%$
5	2	1	9.86×10^{-16}	-1.096	$\pm 4.08\%$	0.003	$\pm 1.09\%$
5	3	1	1.94×10^{-15}	-1.267	$\pm 3.47\%$	-0.001	$\pm 0.13\%$
5	4	1	2.80×10^{-15}	-1.375	$\pm 1.96\%$	-0.007	$\pm 0.78\%$
2	0	3	7.07×10^{-15}	-0.675	$\pm 2.05\%$	-0.001	$\pm 0.20\%$
2	1	3	1.01×10^{-14}	-0.901	$\pm 3.89\%$	0.009	$\pm 4.16\%$
3	0	3	1.51×10^{-15}	-0.696	$\pm 1.63\%$	-0.001	$\pm 0.34\%$
3	1	3	3.63×10^{-15}	-0.873	$\pm 2.50\%$	0.010	$\pm 3.89\%$
3	2	3	8.19×10^{-15}	-1.097	$\pm 3.98\%$	0.002	$\pm 1.01\%$
4	0	3	5.16×10^{-16}	-0.701	$\pm 1.56\%$	-0.001	$\pm 0.46\%$
4	1	3	1.62×10^{-15}	-0.845	$\pm 2.06\%$	0.010	$\pm 3.88\%$
4	2	3	5.19×10^{-15}	-1.078	$\pm 3.73\%$	0.002	$\pm 0.98\%$
4	3	3	6.94×10^{-15}	-1.271	$\pm 3.44\%$	-0.001	$\pm 0.17\%$
5	0	3	2.09×10^{-16}	-0.711	$\pm 1.39\%$	-0.001	$\pm 0.69\%$
5	1	3	8.63×10^{-16}	-0.813	$\pm 1.51\%$	0.010	$\pm 3.88\%$
5	2	3	3.21×10^{-15}	-1.055	$\pm 3.43\%$	0.002	$\pm 0.97\%$
5	3	3	5.83×10^{-15}	-1.267	$\pm 3.47\%$	-0.001	$\pm 0.15\%$
5	4	3	8.39×10^{-15}	-1.375	$\pm 1.96\%$	-0.007	$\pm 0.79\%$

^aSum of transitions to a given level from levels $5 < n < \infty$

^bFor densities below $n_{e,2} = n_e/10^2 = 1$, $\alpha' = \alpha'_4 t^{b_{\alpha'}}$; for densities in the range $n_e = 10^2 - 10^6 \text{ cm}^{-3}$, $\alpha' = \alpha'_4 t^{b_{\alpha'}} n_{e,2}^{c_{\alpha'}}$

^cError over temperature range $t = 0.5 - 2.0$ holding n_e fixed.

^dError over density range $\log n_e = 2 - 6$ holding T_e fixed.

Table 4. Transition data for He I

n_l	l_l	$g_{S,l}$	n_u	l_u	$g_{S,u}$	λ_{ul} (Å)	A_{ul} s^{-1}	Ω_4	b_Ω	e_Ω
1	0	1	2	0	3	626.	1.13×10^{-4}	6.86×10^{-2}	0.020	$\pm 4.09\%$
1	0	1	2	0	1	602.	5.13×10^1	3.60×10^{-2}	0.180	$\pm 2.24\%$
1	0	1	2	1	3	591.	1.76×10^2	2.27×10^{-2}	0.463	$\pm 2.60\%$
1	0	1	2	1	1	584.	1.80×10^9	1.54×10^{-2}	0.631	$\pm 1.88\%$
1	0	1	3	0	3	546.	—	1.60×10^{-2}	0.036	$\pm 3.38\%$
1	0	1	3	0	1	542.	—	8.75×10^{-3}	0.118	$\pm 6.75\%$
1	0	1	3	1	3	540.	—	7.39×10^{-3}	0.324	$\pm 6.37\%$
1	0	1	3	1	1	537.	5.66×10^8	3.72×10^{-3}	0.906	$\pm 9.90\%$
1	0	1	3	2	3	538.	—	2.30×10^{-3}	0.094	$\pm 1.15\%$
1	0	1	3	2	1	538.	—	4.78×10^{-3}	0.071	$\pm 6.66\%$
1	0	1	4	0	3	526.	—	6.90×10^{-3}	0.228	$\pm 2.90\%$
1	0	1	4	0	1	524.	—	3.52×10^{-3}	0.435	$\pm 7.08\%$
1	0	1	4	1	3	524.	—	3.68×10^{-3}	0.539	$\pm 5.64\%$
1	0	1	4	1	1	522.	2.43×10^8	2.23×10^{-3}	1.236	$\pm 6.75\%$
1	0	1	4	2	3	523.	—	1.37×10^{-3}	0.495	$\pm 3.38\%$
1	0	1	4	2	1	523.	—	2.72×10^{-3}	0.627	$\pm 1.96\%$
1	0	1	4	3	3	523.	—	4.90×10^{-4}	0.089	$\pm 1.82\%$
1	0	1	4	3	1	523.	—	7.59×10^{-4}	0.053	$\pm 2.15\%$
1	0	1	5	1	1	516.	1.26×10^8	—	0.000	$\pm 0.00\%$
2	0	1	2	1	3	35649.	—	1.70×10^0	0.094	$\pm 5.72\%$
2	0	1	2	1	1	20589.	1.97×10^6	1.85×10^1	0.719	$\pm 18.44\%$
2	0	1	3	0	3	5905.	—	5.67×10^{-1}	-0.375	$\pm 2.91\%$
2	0	1	3	0	1	5388.	—	6.19×10^{-1}	0.170	$\pm 8.29\%$
2	0	1	3	1	3	5192.	—	5.11×10^{-1}	-0.201	$\pm 3.66\%$
2	0	1	3	1	1	5017.	1.34×10^7	3.44×10^{-1}	0.325	$\pm 1.64\%$
2	0	1	3	2	3	5051.	—	3.33×10^{-1}	0.285	$\pm 1.95\%$
2	0	1	3	2	1	5051.	—	1.22×10^0	0.580	$\pm 7.16\%$
2	0	1	4	0	3	4169.	—	1.96×10^{-1}	-0.190	$\pm 0.66\%$
2	0	1	4	0	1	4060.	—	1.68×10^{-1}	0.326	$\pm 12.15\%$
2	0	1	4	1	3	4015.	—	1.86×10^{-1}	-0.055	$\pm 1.02\%$
2	0	1	4	1	1	3966.	6.95×10^6	1.22×10^{-1}	0.737	$\pm 5.46\%$
2	0	1	4	2	3	3979.	—	1.24×10^{-1}	0.513	$\pm 1.69\%$
2	0	1	4	2	1	3979.	—	3.50×10^{-1}	0.728	$\pm 8.22\%$
2	0	1	4	3	3	3978.	—	8.66×10^{-2}	0.226	$\pm 4.93\%$
2	0	1	4	3	1	3978.	—	2.58×10^{-1}	0.663	$\pm 2.53\%$
2	0	1	5	1	1	3615.	3.80×10^6	3.23×10^{-2}	0.602	$\pm 18.65\%$
2	1	1	3	0	3	8275.	—	1.11×10^0	-0.295	$\pm 2.91\%$
2	1	1	3	0	1	7283.	1.83×10^7	8.68×10^{-1}	0.212	$\pm 6.95\%$
2	1	1	3	1	3	6940.	—	1.18×10^0	-0.126	$\pm 2.91\%$
2	1	1	3	1	1	6643.	—	1.42×10^0	0.638	$\pm 2.44\%$
2	1	1	3	2	3	6691.	—	8.19×10^{-1}	0.330	$\pm 0.46\%$

Table 4—Continued

n_l	l_l	$g_{S,l}$	n_u	l_u	$g_{S,u}$	λ_{ul} (Å)	A_{ul} s^{-1}	Ω_4	b_Ω	e_Ω
	1	1	3	2	1	6680.	6.37×10^7	3.68×10^0	0.731	$\pm 9.75\%$
2	1	1	4	0	3	5226.	—	4.19×10^{-1}	-0.109	$\pm 1.47\%$
2	1	1	4	0	1	5049.	6.77×10^6	3.15×10^{-1}	0.320	$\pm 9.59\%$
2	1	1	4	1	3	4986.	—	4.15×10^{-1}	-0.008	$\pm 2.07\%$
2	1	1	4	1	1	4919.	—	4.46×10^{-1}	0.988	$\pm 4.65\%$
2	1	1	4	2	3	4931.	—	3.14×10^{-1}	0.492	$\pm 1.70\%$
2	1	1	4	2	1	4923.	1.99×10^7	1.16×10^0	0.871	$\pm 8.90\%$
2	1	1	4	3	3	4929.	—	1.85×10^{-1}	0.206	$\pm 2.27\%$
2	1	1	4	3	1	4929.	—	8.13×10^{-1}	0.702	$\pm 4.12\%$
2	1	1	5	0	1	4439.	3.27×10^6	2.99×10^{-2}	0.584	$\pm 14.60\%$
2	1	1	5	2	1	4389.	8.99×10^6	3.87×10^{-1}	0.586	$\pm 14.76\%$
3	0	1	3	1	3	143055.	—	3.08×10^0	-0.324	$\pm 4.89\%$
3	0	1	3	1	1	74405.	2.52×10^5	1.18×10^0	0.927	$\pm 11.00\%$
3	0	1	3	2	3	80953.	—	1.60×10^0	0.012	$\pm 7.86\%$
3	0	1	4	0	3	18432.	—	7.36×10^{-1}	-0.588	$\pm 2.86\%$
3	0	1	4	0	1	16484.	—	2.18×10^0	0.267	$\pm 15.39\%$
3	0	1	4	1	3	15765.	—	9.01×10^{-1}	-0.424	$\pm 2.72\%$
3	0	1	4	1	1	15088.	1.41×10^6	9.79×10^{-1}	0.594	$\pm 10.61\%$
3	0	1	4	2	3	15219.	—	7.57×10^{-1}	-0.210	$\pm 5.04\%$
3	0	1	4	2	1	15214.	—	3.21×10^0	0.441	$\pm 8.40\%$
3	0	1	4	3	3	15201.	—	1.27×10^0	0.081	$\pm 7.87\%$
3	0	1	4	3	1	15201.	—	4.16×10^0	0.603	$\pm 4.12\%$
3	0	1	5	1	1	11016.	9.25×10^5	2.48×10^{-1}	1.230	$\pm 4.28\%$
3	1	1	4	0	3	24490.	—	9.66×10^{-1}	-0.262	$\pm 2.95\%$
3	1	1	4	0	1	21137.	4.59×10^6	2.45×10^0	0.635	$\pm 9.97\%$
3	1	1	4	1	3	19996.	—	1.42×10^0	-0.250	$\pm 4.68\%$
3	1	1	4	1	1	18951.	—	4.21×10^0	0.536	$\pm 8.68\%$
3	1	1	4	2	3	19125.	—	1.40×10^0	-0.008	$\pm 6.85\%$
3	1	1	4	2	1	19091.	7.12×10^6	5.75×10^0	0.455	$\pm 8.30\%$
3	1	1	4	3	3	19098.	—	1.77×10^0	0.186	$\pm 5.21\%$
3	1	1	4	3	1	19098.	—	8.60×10^0	0.379	$\pm 38.16\%$
3	1	1	5	0	1	13414.	2.06×10^6	5.15×10^{-1}	1.121	$\pm 4.82\%$
3	1	1	5	2	1	12972.	3.36×10^6	3.49×10^0	1.146	$\pm 4.81\%$
3	2	1	3	1	1	961553.	1.53×10^2	3.30×10^1	1.377	$\pm 3.56\%$
3	2	1	4	0	3	23882.	—	1.40×10^0	-0.309	$\pm 1.98\%$
3	2	1	4	0	1	20711.	—	2.91×10^0	0.031	$\pm 4.15\%$
3	2	1	4	1	3	19589.	—	2.52×10^0	-0.290	$\pm 3.04\%$
3	2	1	4	1	1	18560.	2.97×10^5	4.85×10^0	0.272	$\pm 5.18\%$
3	2	1	4	2	3	18753.	—	2.54×10^0	-0.049	$\pm 5.08\%$

Table 4—Continued

n_l	l_l	$g_{S,l}$	n_u	l_u	$g_{S,u}$	λ_{ul} (Å)	A_{ul} s^{-1}	Ω_4	b_Ω	e_Ω
	2	1	4	2	1	18746.	—	1.06×10^1	0.237	$\pm 22.14\%$
3	2	1	4	3	3	18727.	—	3.47×10^0	0.076	$\pm 5.53\%$
3	2	1	4	3	1	18701.	1.38×10^7	2.14×10^1	0.696	$\pm 10.62\%$
3	2	1	5	1	1	12758.	1.27×10^5	1.18×10^{-1}	0.977	$\pm 2.94\%$
3	2	1	5	3	1	12793.	4.54×10^6	2.85×10^1	0.777	$\pm 0.78\%$
4	0	1	4	1	3	361512.	—	2.58×10^0	-0.488	$\pm 4.56\%$
4	0	1	4	1	1	180832.	5.83×10^4	2.17×10^1	0.726	$\pm 10.50\%$
4	0	1	4	2	3	198294.	—	1.93×10^0	-0.275	$\pm 8.47\%$
4	0	1	4	3	3	195417.	—	1.95×10^0	-0.248	$\pm 8.60\%$
4	0	1	4	3	1	195417.	—	1.52×10^1	-0.455	$\pm 3.06\%$
4	0	1	5	1	1	33300.	2.93×10^5	6.75×10^0	0.998	$\pm 7.61\%$
4	1	1	5	0	1	46062.	1.50×10^6	5.22×10^1	0.826	$\pm 6.33\%$
4	1	1	5	2	1	41237.	1.52×10^6	1.57×10^2	0.888	$\pm 6.71\%$
4	2	1	4	1	1	2173930.	5.66×10^1	1.55×10^2	1.456	$\pm 1.46\%$
4	2	1	4	3	3	18412769.	—	7.72×10^0	-0.167	$\pm 7.89\%$
4	2	1	4	3	1	18389496.	—	3.83×10^3	1.308	$\pm 4.16\%$
4	2	1	5	1	1	40064.	1.63×10^5	1.05×10^1	0.840	$\pm 6.29\%$
4	2	1	5	3	1	40412.	2.58×10^6	3.54×10^2	0.944	$\pm 1.21\%$
4	3	1	4	3	3	0.	—	1.28×10^1	-0.129	$\pm 6.69\%$
4	3	1	5	2	1	40559.	5.05×10^4	4.93×10^0	0.944	$\pm 1.22\%$
4	3	1	5	4	1	40501.	4.25×10^6	7.48×10^2	0.944	$\pm 1.21\%$
5	0	1	5	1	1	358423.	1.87×10^4	1.88×10^3	0.839	$\pm 5.65\%$
5	2	1	5	1	1	3999952.	2.39×10^1	1.75×10^4	0.372	$\pm 1.68\%$
5	2	1	5	3	1	28407512.	—	4.54×10^4	0.477	$\pm 3.83\%$
5	4	1	5	3	1	1.	—	2.68×10^4	0.403	$\pm 2.39\%$
2	0	3	2	0	1	15593.	—	2.39×10^0	-0.018	$\pm 8.35\%$
2	0	3	2	1	3	10833.	1.02×10^7	2.69×10^1	0.812	$\pm 2.70\%$
2	0	3	2	1	1	8878.	—	9.74×10^{-1}	0.241	$\pm 7.06\%$
2	0	3	3	0	3	4283.	—	2.39×10^0	-0.045	$\pm 4.84\%$
2	0	3	3	0	1	4004.	—	3.84×10^{-1}	-0.242	$\pm 2.48\%$
2	0	3	3	1	3	3890.	9.47×10^6	1.76×10^0	0.019	$\pm 2.70\%$
2	0	3	3	1	1	3800.	—	1.57×10^{-1}	0.176	$\pm 5.59\%$
2	0	3	3	2	3	3815.	—	2.07×10^0	0.636	$\pm 3.70\%$
2	0	3	3	2	1	3815.	—	3.08×10^{-1}	0.034	$\pm 1.86\%$
2	0	3	4	0	3	3289.	—	7.48×10^{-1}	0.132	$\pm 4.78\%$
2	0	3	4	0	1	3222.	—	1.32×10^{-1}	-0.091	$\pm 2.18\%$
2	0	3	4	1	3	3189.	5.63×10^6	6.23×10^{-1}	0.204	$\pm 6.27\%$
2	0	3	4	1	1	3165.	—	6.39×10^{-2}	0.450	$\pm 5.82\%$

Table 4—Continued

n_l	l_l	$g_{S,l}$	n_u	l_u	$g_{S,u}$	λ_{ul} (Å)	A_{ul} s^{-1}	Ω_4	b_Ω	e_Ω
	0	3	4	2	3	3170.	—	7.33×10^{-1}	0.873	$\pm 3.85\%$
2	0	3	4	2	1	3170.	—	1.28×10^{-1}	0.354	$\pm 1.48\%$
2	0	3	4	3	3	3169.	—	5.05×10^{-1}	0.501	$\pm 2.03\%$
2	0	3	4	3	1	3169.	—	5.05×10^{-2}	0.124	$\pm 2.59\%$
2	0	3	5	1	3	2946.	3.20×10^6	5.41×10^{-2}	0.281	$\pm 26.31\%$
2	1	3	2	1	1	48896.	—	2.07×10^0	0.411	$\pm 6.85\%$
2	1	3	3	0	3	7067.	2.78×10^7	5.70×10^0	0.018	$\pm 6.67\%$
2	1	3	3	0	1	6347.	—	6.93×10^{-1}	-0.187	$\pm 3.10\%$
2	1	3	3	1	3	6077.	—	8.06×10^0	0.251	$\pm 4.71\%$
2	1	3	3	1	1	5849.	—	5.74×10^{-1}	0.204	$\pm 9.03\%$
2	1	3	3	2	3	5877.	7.07×10^7	7.74×10^0	0.867	$\pm 5.91\%$
2	1	3	3	2	1	5884.	—	8.62×10^{-1}	0.074	$\pm 3.77\%$
2	1	3	4	0	3	4715.	9.52×10^6	1.72×10^0	0.156	$\pm 3.80\%$
2	1	3	4	0	1	4582.	—	3.17×10^{-1}	-0.089	$\pm 1.09\%$
2	1	3	4	1	3	4525.	—	2.81×10^0	0.430	$\pm 7.75\%$
2	1	3	4	1	1	4469.	—	1.94×10^{-1}	0.491	$\pm 6.61\%$
2	1	3	4	2	3	4473.	2.46×10^7	2.72×10^0	0.961	$\pm 5.53\%$
2	1	3	4	2	1	4478.	—	3.21×10^{-1}	0.275	$\pm 4.95\%$
2	1	3	4	3	3	4477.	—	2.18×10^0	0.619	$\pm 2.86\%$
2	1	3	4	3	1	4477.	—	1.56×10^{-1}	0.185	$\pm 0.91\%$
2	1	3	5	0	3	4122.	4.45×10^6	1.10×10^{-1}	0.471	$\pm 17.08\%$
2	1	3	5	2	3	4027.	1.16×10^7	1.27×10^0	0.472	$\pm 17.53\%$
3	0	3	3	0	1	61510.	—	2.81×10^0	-0.444	$\pm 4.84\%$
3	0	3	3	1	3	42955.	1.07×10^6	5.95×10^1	0.000	$\pm 0.02\%$
3	0	3	3	1	1	33694.	—	1.46×10^0	-0.079	$\pm 7.17\%$
3	0	3	3	2	3	34952.	—	6.38×10^1	0.000	$\pm 0.00\%$
3	0	3	3	2	1	34916.	—	2.67×10^0	-0.235	$\pm 3.06\%$
3	0	3	4	0	3	14182.	—	7.70×10^0	0.111	$\pm 12.08\%$
3	0	3	4	0	1	13000.	—	5.37×10^{-1}	-0.509	$\pm 1.40\%$
3	0	3	4	1	3	12531.	7.09×10^5	6.67×10^0	0.304	$\pm 8.94\%$
3	0	3	4	1	1	12129.	—	3.13×10^{-1}	-0.072	$\pm 3.71\%$
3	0	3	4	2	3	12200.	—	5.74×10^0	0.412	$\pm 1.16\%$
3	0	3	4	2	1	12197.	—	9.01×10^{-1}	-0.264	$\pm 4.25\%$
3	0	3	4	3	3	12189.	—	1.25×10^1	0.545	$\pm 4.11\%$
3	0	3	4	3	1	12189.	—	1.07×10^0	0.100	$\pm 8.30\%$
3	0	3	5	1	3	9466.	5.69×10^5	2.72×10^{-1}	1.206	$\pm 2.68\%$
3	1	3	3	1	1	155496.	—	3.43×10^0	0.114	$\pm 5.83\%$
3	1	3	3	2	3	186220.	1.29×10^4	1.84×10^1	0.717	$\pm 9.32\%$
3	1	3	3	2	1	185442.	—	6.96×10^0	-0.176	$\pm 3.70\%$

Table 4—Continued

n_l	l_l	$g_{S,l}$	n_u	l_u	$g_{S,u}$	λ_{ul} (Å)	A_{ul} s^{-1}	Ω_4	b_Ω	e_Ω
	1	3	4	0	3	21128.	6.51×10^6	1.48×10^1	0.463	$\pm 5.25\%$
3	1	3	4	0	1	18630.	—	9.72×10^{-1}	-0.370	$\pm 2.42\%$
3	1	3	4	1	3	17717.	—	1.98×10^1	0.251	$\pm 5.72\%$
3	1	3	4	1	1	16893.	—	1.05×10^0	-0.101	$\pm 6.94\%$
3	1	3	4	2	3	17007.	6.19×10^6	1.71×10^1	0.330	$\pm 5.51\%$
3	1	3	4	2	1	17025.	—	2.08×10^0	-0.182	$\pm 5.55\%$
3	1	3	4	3	3	17009.	—	2.98×10^1	0.385	$\pm 38.87\%$
3	1	3	4	3	1	17009.	—	1.88×10^0	0.177	$\pm 4.84\%$
3	1	3	5	0	3	12850.	2.73×10^6	1.89×10^0	1.095	$\pm 4.24\%$
3	1	3	5	2	3	11973.	3.48×10^6	8.11×10^0	1.146	$\pm 4.25\%$
3	2	3	3	1	1	935906.	—	3.61×10^0	0.153	$\pm 9.06\%$
3	2	3	3	2	1	33375619.	—	6.93×10^0	0.100	$\pm 3.86\%$
3	2	3	4	0	3	23865.	—	1.45×10^1	0.008	$\pm 2.80\%$
3	2	3	4	0	1	20698.	—	1.01×10^0	-0.289	$\pm 1.99\%$
3	2	3	4	1	3	19550.	6.46×10^5	2.28×10^1	0.126	$\pm 4.03\%$
3	2	3	4	1	1	18575.	—	1.24×10^0	-0.009	$\pm 7.09\%$
3	2	3	4	2	3	18742.	—	3.53×10^1	0.240	$\pm 22.42\%$
3	2	3	4	2	1	18735.	—	2.72×10^0	-0.075	$\pm 3.82\%$
3	2	3	4	3	3	18690.	1.38×10^7	6.37×10^1	0.630	$\pm 10.88\%$
3	2	3	4	3	1	18716.	—	3.24×10^0	0.062	$\pm 4.69\%$
3	2	3	5	1	3	12989.	2.73×10^5	8.36×10^{-1}	0.966	$\pm 2.99\%$
3	2	3	5	3	3	12789.	4.54×10^6	8.55×10^1	0.777	$\pm 0.78\%$
4	0	3	4	0	1	155979.	—	2.27×10^0	-0.608	$\pm 3.76\%$
4	0	3	4	1	3	108814.	2.28×10^5	6.38×10^1	0.636	$\pm 10.87\%$
4	0	3	4	1	1	83798.	—	1.08×10^0	-0.214	$\pm 8.54\%$
4	0	3	4	2	1	87153.	—	2.50×10^0	-0.352	$\pm 7.17\%$
4	0	3	4	3	3	86742.	—	4.49×10^1	-0.316	$\pm 2.87\%$
4	0	3	4	3	1	86742.	—	2.06×10^0	-0.223	$\pm 8.49\%$
4	0	3	5	1	3	28547.	1.21×10^5	4.56×10^0	1.034	$\pm 7.57\%$
4	1	3	4	1	1	362822.	—	3.58×10^0	-0.086	$\pm 12.03\%$
4	1	3	4	2	3	438594.	4.18×10^3	8.29×10^1	0.890	$\pm 8.62\%$
4	1	3	4	2	1	435388.	—	6.83×10^0	-0.342	$\pm 7.40\%$
4	1	3	4	3	1	425330.	—	5.38×10^0	-0.281	$\pm 7.45\%$
4	1	3	5	0	3	46948.	2.02×10^6	2.48×10^2	0.792	$\pm 5.95\%$
4	1	3	5	2	3	37037.	1.28×10^6	2.53×10^2	0.925	$\pm 6.96\%$
4	2	3	4	1	1	2086257.	—	3.82×10^0	-0.145	$\pm 10.09\%$
4	2	3	4	2	1	50103835.	—	7.66×10^0	-0.127	$\pm 8.77\%$
4	2	3	4	3	3	13446410.	—	7.57×10^3	1.355	$\pm 3.74\%$

Table 4—Continued

n_l	l_l	$g_{S,l}$	n_u	l_u	$g_{S,u}$	λ_{ul} (Å)	A_{ul} s^{-1}	Ω_4	b_Ω	e_Ω
	2	3	4	3	1	13464625.	—	7.79×10^0	-0.173	$\pm 7.65\%$
4	2	3	5	1	3	42445.	3.27×10^5	8.31×10^1	0.810	$\pm 6.04\%$
4	2	3	5	3	3	40379.	2.58×10^6	1.06×10^3	0.944	$\pm 1.21\%$
4	3	3	4	1	1	2468778.	—	4.02×10^0	-0.185	$\pm 9.49\%$
4	3	3	5	2	3	40575.	5.05×10^4	1.48×10^1	0.944	$\pm 1.22\%$
4	3	3	5	4	3	40501.	4.25×10^6	2.24×10^3	0.944	$\pm 1.21\%$
5	0	3	5	1	3	220265.	7.02×10^4	3.39×10^3	0.925	$\pm 5.23\%$
5	1	3	5	2	3	862068.	1.51×10^3	2.37×10^4	0.604	$\pm 4.96\%$
5	2	3	5	3	3	22121278.	—	1.22×10^5	0.440	$\pm 3.29\%$
5	4	3	5	3	3	1.	—	8.04×10^4	0.403	$\pm 2.39\%$

Table 5. He I Emission Line Intensities ($n_e = 10^2 \text{ cm}^{-3}$)^a

$T =$	5000	10,000	20,000	a_j	b_j	c_j	e_j
$4\pi j_{H\beta}/n_e n_{H^+}$ ^{b,c}	2.20×10^{-25}	1.23×10^{-25}	6.58×10^{-26}	1.37×10^{-25}	-0.982	-0.104	$\pm 0.66\%$
$4\pi j_{4686}/n_e n_{He^{++}}$ ^{b,c}	3.02×10^{-24}	1.52×10^{-24}	7.29×10^{-25}	1.65×10^{-24}	-1.118	-0.087	$\pm 0.63\%$
$4\pi j_{Br\gamma}/n_e n_{H^+}$ ^{b,c}	2.13×10^{-25}	1.15×10^{-25}	5.82×10^{-26}	1.31×10^{-25}	-1.077	-0.133	$\pm 0.72\%$
$4\pi j_{4473}/n_e n_{He^+}$ ^b	1.18×10^{-25}	6.16×10^{-26}	3.11×10^{-26}	6.68×10^{-26}	-1.048	-0.080	$\pm 0.65\%$
j_{2946}/j_{4473}	0.356	0.438	0.540	2.91×10^{-26}	-0.740	-0.076	$\pm 0.65\%$
j_{3189}/j_{4473}	0.745	0.913	1.136	5.90×10^{-26}	-0.707	-0.048	$\pm 0.57\%$
j_{3615}/j_{4473}	0.094	0.110	0.127	7.60×10^{-27}	-0.864	-0.115	$\pm 0.52\%$
j_{3890}/j_{4473}	1.864	2.231	2.742	1.41×10^{-25}	-0.709	-0.025	$\pm 0.58\%$
j_{3966}/j_{4473}	0.193	0.226	0.261	1.53×10^{-26}	-0.845	-0.097	$\pm 0.52\%$
j_{4027}/j_{4473}	0.450	0.464	0.463	3.32×10^{-26}	-1.098	-0.148	$\pm 0.75\%$
j_{4122}/j_{4473} [*]	0.028	0.040	0.059	2.39×10^{-27}	-0.405	0.024	$\pm 0.53\%$
j_{4389}/j_{4473}	0.120	0.123	0.121	8.83×10^{-27}	-1.121	-0.156	$\pm 0.53\%$
j_{4439}/j_{4473}	0.013	0.017	0.023	1.06×10^{-27}	-0.547	-0.011	$\pm 0.51\%$
j_{4473}/j_{4473}	1.000	1.000	1.000	6.68×10^{-26}	-1.048	-0.080	$\pm 0.65\%$
j_{4715}/j_{4473}	0.075	0.105	0.164	5.52×10^{-27}	-0.230	0.155	$\pm 0.88\%$
j_{4923}/j_{4473}	0.269	0.266	0.257	1.85×10^{-26}	-1.125	-0.124	$\pm 0.52\%$
j_{5017}/j_{4473}	0.496	0.567	0.646	3.79×10^{-26}	-0.859	-0.083	$\pm 0.52\%$
j_{5049}/j_{4473}	0.031	0.041	0.057	2.42×10^{-27}	-0.489	0.035	$\pm 0.51\%$
j_{5877}/j_{4473}	2.989	2.743	2.591	1.73×10^{-25}	-1.091	-0.024	$\pm 0.76\%$
j_{6680}/j_{4473}	0.857	0.778	0.702	5.25×10^{-26}	-1.202	-0.091	$\pm 0.51\%$
j_{7067}/j_{4473}	0.358	0.481	0.713	2.65×10^{-26}	-0.340	0.114	$\pm 0.68\%$
j_{7283}/j_{4473}	0.114	0.146	0.197	8.88×10^{-27}	-0.547	0.015	$\pm 0.52\%$
j_{9466}/j_{4473}	0.020	0.024	0.030	1.61×10^{-27}	-0.740	-0.076	$\pm 0.65\%$
j_{10833}/j_{4473}	4.298	5.515	7.895	2.94×10^{-25}	-0.364	0.144	$\pm 0.98\%$
j_{11973}/j_{4473}	0.045	0.047	0.047	3.35×10^{-27}	-1.098	-0.148	$\pm 0.76\%$
j_{12531}/j_{4473}	0.024	0.029	0.036	1.89×10^{-27}	-0.707	-0.048	$\pm 0.57\%$
j_{12789}/j_{4473}	0.174	0.152	0.129	1.08×10^{-26}	-1.331	-0.141	$\pm 0.69\%$
j_{12793}/j_{4473}	0.058	0.051	0.043	3.60×10^{-27}	-1.331	-0.141	$\pm 0.52\%$
j_{12972}/j_{4473}	0.015	0.016	0.015	1.12×10^{-27}	-1.121	-0.156	$\pm 0.53\%$
j_{15088}/j_{4473}	0.010	0.012	0.014	8.14×10^{-28}	-0.845	-0.097	$\pm 0.52\%$
j_{17007}/j_{4473}	0.066	0.066	0.066	4.42×10^{-27}	-1.048	-0.080	$\pm 0.65\%$
j_{18690}/j_{4473}	0.440	0.360	0.295	2.40×10^{-26}	-1.332	-0.078	$\pm 0.55\%$
j_{18701}/j_{4473}	0.146	0.120	0.097	8.16×10^{-27}	-1.364	-0.100	$\pm 0.51\%$
j_{19091}/j_{4473}	0.025	0.025	0.024	1.71×10^{-27}	-1.125	-0.123	$\pm 0.52\%$
j_{19550}/j_{4473}	0.014	0.017	0.021	1.10×10^{-27}	-0.707	-0.048	$\pm 0.57\%$
j_{20589}/j_{4473}	0.629	0.670	0.721	4.35×10^{-26}	-0.919	-0.054	$\pm 0.52\%$
j_{21128}/j_{4473}	0.011	0.016	0.025	8.43×10^{-28}	-0.230	0.155	$\pm 0.88\%$

^aFits given by $4\pi j_{\text{line}}/n_e n_{He^+} = a_j t^{b_j} \exp(c_j/t)$, with maximum error $\pm e_j\%$ over interval $t = 0.5 - 2.0$.

^bEmission coefficient in units $\text{ergs s}^{-1}\text{cm}^3$

^cFrom Storey & Hummer (1995)

*Flux may be enhanced more than 5 % for $t \geq 1.5$ due to collisional excitation to $n = 5$ levels. See §3.1

Table 6. He I Emission Line Intensities ($n_e = 10^4 \text{ cm}^{-3}$)^a

$T =$	5000	10,000	20,000	a_j	b_j	c_j	e_j
$4\pi j_{H\beta}/n_e n_{H^+}$ ^{b,c}	2.22×10^{-25}	1.24×10^{-25}	6.59×10^{-26}	1.36×10^{-25}	-0.979	-0.095	$\pm 0.69\%$
$4\pi j_{4686}/n_e n_{He^{++}}$ ^{b,c}	2.96×10^{-24}	1.49×10^{-24}	7.22×10^{-25}	1.63×10^{-24}	-1.110	-0.086	$\pm 0.64\%$
$4\pi j_{Br\gamma}/n_e n_{H^+}$ ^{b,c}	2.14×10^{-25}	1.15×10^{-25}	5.81×10^{-26}	1.31×10^{-25}	-1.078	-0.127	$\pm 0.70\%$
$4\pi j_{4473}/n_e n_{He^+}$ ^b	1.18×10^{-25}	6.52×10^{-26}	5.07×10^{-26}	3.36×10^{-26}	0.092	0.665	$\pm 3.72\%$
j_{2946}/j_{4473} [†]	0.357	0.419	0.359	2.62×10^{-26}	-0.563	0.043	$\pm 0.88\%$
j_{3189}/j_{4473}	0.748	0.931	0.997	4.13×10^{-26}	0.011	0.385	$\pm 1.60\%$
j_{3615}/j_{4473} [*]	0.094	0.104	0.078	7.61×10^{-27}	-0.864	-0.111	$\pm 0.52\%$
j_{3890}/j_{4473}	1.891	2.555	2.953	1.14×10^{-25}	0.129	0.380	$\pm 1.85\%$
j_{3966}/j_{4473}	0.194	0.219	0.187	1.28×10^{-26}	-0.516	0.113	$\pm 0.55\%$
j_{4027}/j_{4473} [†]	0.450	0.440	0.284	3.31×10^{-26}	-1.097	-0.144	$\pm 0.76\%$
j_{4122}/j_{4473} [†]	0.028	0.037	0.036	2.36×10^{-27}	-0.391	0.037	$\pm 0.52\%$
j_{4389}/j_{4473} [*]	0.120	0.116	0.074	8.81×10^{-27}	-1.120	-0.151	$\pm 0.53\%$
j_{4439}/j_{4473}	0.013	0.016	0.014	1.05×10^{-27}	-0.546	-0.007	$\pm 0.51\%$
j_{4473}/j_{4473}	1.000	1.000	1.000	3.36×10^{-26}	0.092	0.665	$\pm 3.72\%$
j_{4715}/j_{4473}	0.076	0.146	0.291	4.25×10^{-27}	1.251	0.805	$\pm 5.07\%$
j_{4923}/j_{4473}	0.269	0.259	0.196	1.40×10^{-26}	-0.634	0.192	$\pm 0.60\%$
j_{5017}/j_{4473}	0.498	0.572	0.503	3.19×10^{-26}	-0.432	0.157	$\pm 0.55\%$
j_{5049}/j_{4473}	0.031	0.045	0.059	1.84×10^{-27}	0.381	0.479	$\pm 0.72\%$
j_{5877}/j_{4473}	2.966	2.933	3.118	8.42×10^{-26}	0.304	0.821	$\pm 3.24\%$
j_{6680}/j_{4473}	0.849	0.775	0.554	4.17×10^{-26}	-0.712	0.192	$\pm 0.56\%$
j_{7067}/j_{4473}	0.398	0.943	1.525	6.49×10^{-26}	0.323	-0.053	$\pm 4.15\%$
j_{7283}/j_{4473}	0.118	0.196	0.236	1.19×10^{-26}	-0.012	0.072	$\pm 0.81\%$
j_{9466}/j_{4473} [*]	0.020	0.023	0.020	1.45×10^{-27}	-0.563	0.043	$\pm 0.88\%$
j_{10833}/j_{4473}	12.910	31.393	40.743	3.58×10^{-24}	-0.383	-0.558	$\pm 2.83\%$
j_{11973}/j_{4473} [†]	0.045	0.044	0.029	3.34×10^{-27}	-1.097	-0.144	$\pm 0.76\%$
j_{12531}/j_{4473}	0.024	0.030	0.032	1.32×10^{-27}	0.011	0.385	$\pm 1.60\%$
j_{12789}/j_{4473} [†]	0.173	0.143	0.079	1.07×10^{-26}	-1.328	-0.138	$\pm 0.69\%$
j_{12793}/j_{4473}	0.058	0.048	0.026	3.58×10^{-27}	-1.328	-0.138	$\pm 0.52\%$
j_{12972}/j_{4473} [*]	0.015	0.015	0.009	1.12×10^{-27}	-1.120	-0.151	$\pm 0.53\%$
j_{15088}/j_{4473}	0.010	0.012	0.010	6.79×10^{-28}	-0.516	0.113	$\pm 0.55\%$
j_{17007}/j_{4473}	0.066	0.066	0.066	2.22×10^{-27}	0.092	0.665	$\pm 3.72\%$
j_{18690}/j_{4473}	0.429	0.347	0.239	1.59×10^{-26}	-0.663	0.353	$\pm 2.33\%$
j_{18701}/j_{4473}	0.143	0.113	0.064	7.32×10^{-27}	-1.192	0.006	$\pm 0.53\%$
j_{19091}/j_{4473}	0.025	0.024	0.018	1.29×10^{-27}	-0.634	0.192	$\pm 0.60\%$
j_{19550}/j_{4473}	0.014	0.017	0.019	7.72×10^{-28}	0.011	0.385	$\pm 1.60\%$
j_{20589}/j_{4473}	0.758	1.036	0.899	8.35×10^{-26}	-0.708	-0.212	$\pm 0.65\%$
j_{21128}/j_{4473}	0.012	0.022	0.044	6.49×10^{-28}	1.251	0.805	$\pm 5.07\%$

^aFits given by $4\pi j_{\text{line}}/n_e n_{He^+} = a_j t^{b_j} \exp(c_j/t)$, with maximum error $\pm e_j\%$ over interval $t = 0.5 - 2.0$.

^bEmission coefficient in units $\text{ergs s}^{-1}\text{cm}^3$

^cFrom Storey & Hummer (1995)

^{*}Flux may be enhanced more than 5 % for $t \geq 1.5$ due to collisional excitation to $n = 5$ levels. See §3.1

[†]Flux may be enhanced more than 25 % for $t \geq 1.5$ due to collisional excitation to $n = 5$ levels. See §3.1

Table 7. He I Emission Line Intensities ($n_e = 10^6 \text{ cm}^{-3}$)^a

$T =$	5000	10,000	20,000	a_j	b_j	c_j	e_j
$4\pi j_{H\beta}/n_e n_{H^+}$ ^{b,c}	2.29×10^{-25}	1.26×10^{-25}	6.61×10^{-26}	1.36×10^{-25}	-0.979	-0.078	$\pm 0.67\%$
$4\pi j_{4686}/n_e n_{He^{++}}$ ^{b,c}	2.84×10^{-24}	1.44×10^{-24}	7.04×10^{-25}	1.56×10^{-24}	-1.091	-0.079	$\pm 0.64\%$
$4\pi j_{Br\gamma}/n_e n_{H^+}$ ^{b,c}	2.17×10^{-25}	1.15×10^{-25}	5.76×10^{-26}	1.27×10^{-25}	-1.065	-0.102	$\pm 0.70\%$
$4\pi j_{4473}/n_e n_{He^+}$ ^b	1.21×10^{-25}	6.70×10^{-26}	5.58×10^{-26}	3.03×10^{-26}	0.286	0.793	$\pm 4.02\%$
j_{2946}/j_{4473} [†]	0.361	0.417	0.335	2.57×10^{-26}	-0.525	0.082	$\pm 0.94\%$
j_{3189}/j_{4473} [*]	0.759	0.943	0.981	4.01×10^{-26}	0.120	0.454	$\pm 1.59\%$
j_{3615}/j_{4473} [*]	0.096	0.104	0.072	7.61×10^{-27}	-0.863	-0.092	$\pm 0.52\%$
j_{3890}/j_{4473}	1.929	2.677	2.991	1.22×10^{-25}	0.189	0.388	$\pm 2.30\%$
j_{3966}/j_{4473}	0.197	0.219	0.178	1.24×10^{-26}	-0.448	0.169	$\pm 0.56\%$
j_{4027}/j_{4473} [†]	0.452	0.432	0.259	3.29×10^{-26}	-1.095	-0.128	$\pm 0.75\%$
j_{4122}/j_{4473} [†]	0.028	0.036	0.033	2.31×10^{-27}	-0.382	0.055	$\pm 0.52\%$
j_{4389}/j_{4473} [*]	0.121	0.114	0.068	8.76×10^{-27}	-1.117	-0.134	$\pm 0.53\%$
j_{4439}/j_{4473}	0.013	0.016	0.013	1.04×10^{-27}	-0.542	0.009	$\pm 0.51\%$
j_{4473}/j_{4473}	1.000	1.000	1.000	3.03×10^{-26}	0.286	0.793	$\pm 4.02\%$
j_{4715}/j_{4473}	0.077	0.159	0.309	5.15×10^{-27}	1.263	0.726	$\pm 5.81\%$
j_{4923}/j_{4473}	0.269	0.258	0.189	1.32×10^{-26}	-0.524	0.269	$\pm 0.62\%$
j_{5017}/j_{4473}	0.505	0.578	0.486	3.16×10^{-26}	-0.363	0.201	$\pm 0.77\%$
j_{5049}/j_{4473}	0.031	0.047	0.060	1.90×10^{-27}	0.471	0.503	$\pm 0.78\%$
j_{5877}/j_{4473}	2.916	2.972	3.186	8.03×10^{-26}	0.484	0.908	$\pm 3.12\%$
j_{6680}/j_{4473}	0.834	0.769	0.536	4.03×10^{-26}	-0.607	0.247	$\pm 0.56\%$
j_{7067}/j_{4473}	0.429	1.095	1.639	9.25×10^{-26}	0.182	-0.232	$\pm 3.91\%$
j_{7283}/j_{4473}	0.121	0.212	0.243	1.45×10^{-26}	-0.051	-0.018	$\pm 0.85\%$
j_{9466}/j_{4473} [†]	0.020	0.023	0.019	1.42×10^{-27}	-0.525	0.082	$\pm 0.94\%$
j_{10833}/j_{4473}	19.346	39.911	45.367	3.85×10^{-24}	-0.332	-0.365	$\pm 3.05\%$
j_{11973}/j_{4473} [†]	0.046	0.044	0.026	3.32×10^{-27}	-1.095	-0.128	$\pm 0.75\%$
j_{12531}/j_{4473} [*]	0.024	0.030	0.031	1.28×10^{-27}	0.120	0.454	$\pm 1.59\%$
j_{12789}/j_{4473} [†]	0.170	0.139	0.071	1.06×10^{-26}	-1.318	-0.125	$\pm 0.69\%$
j_{12793}/j_{4473}	0.057	0.046	0.024	3.52×10^{-27}	-1.318	-0.125	$\pm 0.52\%$
j_{12972}/j_{4473}	0.015	0.014	0.009	1.11×10^{-27}	-1.117	-0.134	$\pm 0.53\%$
j_{15088}/j_{4473}	0.010	0.012	0.009	6.59×10^{-28}	-0.448	0.169	$\pm 0.56\%$
j_{17007}/j_{4473}	0.066	0.066	0.066	2.01×10^{-27}	0.286	0.794	$\pm 4.02\%$
j_{18690}/j_{4473} [*]	0.411	0.335	0.229	1.44×10^{-26}	-0.510	0.443	$\pm 2.57\%$
j_{18701}/j_{4473}	0.137	0.108	0.058	6.95×10^{-27}	-1.129	0.042	$\pm 0.54\%$
j_{19091}/j_{4473}	0.025	0.024	0.017	1.22×10^{-27}	-0.524	0.269	$\pm 0.62\%$
j_{19550}/j_{4473} [*]	0.014	0.018	0.018	7.50×10^{-28}	0.120	0.454	$\pm 1.59\%$
j_{20589}/j_{4473}	0.875	1.217	0.978	1.07×10^{-25}	-0.755	-0.269	$\pm 0.72\%$
j_{21128}/j_{4473}	0.012	0.024	0.047	7.86×10^{-28}	1.263	0.726	$\pm 5.81\%$

^aFits given by $4\pi j_{\text{line}}/n_e n_{He^+} = a_j t^{b_j} \exp(c_j/t)$, with maximum error $\pm e_j\%$ over interval $t = 0.5 - 2.0$.

^bEmission coefficient in units $\text{ergs s}^{-1}\text{cm}^3$

^cFrom Storey & Hummer (1995)

^{*}Flux may be enhanced more than 5 % for $t \geq 1.5$ due to collisional excitation to $n = 5$ levels. See §3.1

[†]Flux may be enhanced more than 25 % for $t \geq 1.5$ due to collisional excitation to $n = 5$ levels. See §3.1

Table 8. Populations of metastable 2^3S and 2^1S and resultant collisional contributions ($T = 20,000\text{ K}$)^a

$\log n_e =$	2		4		6	
	BSS ^b	KF ^c	BSS	KF	BSS	KF
$n(2^3S)/n_{He^+}$	1.03×10^{-7}	1.06×10^{-7}	2.04×10^{-6}	2.02×10^{-6}	2.53×10^{-6}	2.46×10^{-6}
$C/R(3890.)$	0.042	0.043	0.828	0.815	1.022	0.994
$C/R(3189.)$	0.023	—	0.463	—	0.571	—
$C/R(2946.)$	0.004	—	0.085	—	0.105	—
$C/R(7067.)$	0.152	0.153	3.024	2.898	3.763	3.532
$C/R(5877.)$	0.054	0.055	1.077	1.043	1.343	1.271
$C/R(4715.)$	0.112	—	2.223	—	2.777	—
$C/R(4473.)$	0.035	0.038	0.688	0.712	0.853	0.868
$C/R(4027.)$ ^d	—	0.019	—	0.358	—	0.436
$C/R(18690.)$	0.018	—	0.355	—	0.448	—
$n(2^1S)/n_{He^+}$ ^e	7.57×10^{-14}	—	2.32×10^{-11}	—	2.71×10^{-9}	—
$C/R(5017.)$	0.015	—	0.287	—	0.359	—
$C/R(3966.)$	0.009	—	0.175	—	0.218	—
$C/R(7283.)$	0.054	0.052	1.063	0.991	1.338	1.208
$C/R(6680.)$	0.016	0.016	0.313	0.308	0.402	0.375
$C/R(4923.)$	0.013	0.014	0.262	0.267	0.331	0.325
$C/R(4389.)$	—	0.011	—	0.204	—	0.248
$C/R(18701.)$	0.004	—	0.082	—	0.107	—

^aOnly lines with collisional corrections, C/R, greater than 1% over the density range are shown.

^bCurrent work.

^cFrom Kingdon & Ferland (1995).

^d 2^1S population not estimated in Kingdon & Ferland (1995).

^eCollisions to $n = 5$ not included in current work. See §3.1.

Table 9. Fitting formulae for primordial helium abundance^a

Line	Formula	σ_{atomic}/f	σ_{fit}	Max Error ^b
4686Å	$f = 0.0816t^{0.145}$	—	8.72×10^{-5}	0.25%
6678Å	$f = 2.58t^{0.249+2.0 \times 10^{-4}n_e}$	0.013	3.05×10^{-3}	0.29%
4471Å	$f = 2.01t^{0.127-4.1 \times 10^{-4}n_e}$	0.013	7.67×10^{-3}	0.93%
5876Å	$f = 0.735t^{0.230-6.3 \times 10^{-4}n_e}$	0.015	3.06×10^{-3}	1.02%

^aHelium number abundance is $y = r_{line}f(n_e, t)$, where $f = At^{B_0+B_1n_e}$. Valid over the regime $1.2 < t < 2.0$ and $1 < n_e < 300cm^{-3}$.

^bMaximum difference between calculated value of f and the fitting function.

Table 10. Quantum defects used for energy levels

Term=	S		P		D	
	n_{top}^a	d^b	n_{top}	d	n_{top}	d
Singlet	15	0.140	20	-0.012	18	0.001
Triplet	17	0.297	22	0.068	21	0.003

^aTop level for which energy levels are given by Martin (1973)

^bAdopted quantum defect. See Appendix A.